

NASA
TP
1500
c.1

NASA Technical Paper 1500

LOAN COPY RETURN
AFWL TECHNICAL LIBR
KIRTLAND AFB, N. M.

0134720



TECH LIBRARY KAFB, NM

Estimation of Attainable Leading-Edge Thrust for Wings at Subsonic and Supersonic Speeds

Harry W. Carlson, Robert J. Mack,
and Raymond L. Barger

OCTOBER 1979

NASA



NASA Technical Paper 1500

Estimation of Attainable
Leading-Edge Thrust for Wings
at Subsonic and Supersonic Speeds

Harry W. Carlson, Robert J. Mack,
and Raymond L. Barger
*Langley Research Center
Hampton, Virginia*



National Aeronautics
and Space Administration

**Scientific and Technical
Information Branch**

1979

SUMMARY

A study has been made of the factors which place limits on the theoretical leading-edge thrust, and an empirical method for estimating attainable thrust has been developed. The method is based on the use of simple sweep theory to permit a two-dimensional analysis, the use of theoretical airfoil programs to define thrust dependence on local geometric characteristics, and the examination of experimental two-dimensional airfoil data to define limitations imposed by local Mach numbers and Reynolds numbers. The applicability of the method was demonstrated by comparisons of theoretical and experimental aerodynamic characteristics for a series of wing-body configurations. Generally, good predictions of the attainable thrust and its influence on lift and drag characteristics were obtained over a range of Mach numbers from 0.24 to 1.3.

The method is compatible with the Polhamus leading-edge suction analogy for fully detected vortex flow, when the analogy is considered to represent the limiting condition of a gradual rotation of the suction vector as leading-edge thrust is lost. An additional advantage of the method is the possibility it presents for designing wings in an iterative manner to maximize thrust and the attendant performance benefits.

INTRODUCTION

Leading-edge thrust is an important but little understood aerodynamic phenomena that can have a large influence on wing aerodynamic performance. This force results from the high local velocities and the accompanying low pressures which occur as air flows from a stagnation point on the undersurface of the wing around the leading edge to the upper surface. At low subsonic speeds, the high aerodynamic efficiency of uncambered wings with high aspect ratios depends directly on the presence of leading-edge thrust to counteract the drag arising from pressure forces acting on the remainder of the airfoil. Leading-edge thrust tends to diminish with increasing speeds, but may be present to some degree even in the supersonic speed regime, provided the leading edge is swept behind the Mach angle.

Leading-edge thrust for subsonic speeds may be predicted by a variety of methods including a vortex-lattice computer program (ref. 1) capable of handling wings of complex planform. At supersonic speeds, leading-edge thrust for wings with straight leading edges may be determined by purely analytic means (e.g., ref. 2). A recently developed computer method (ref. 3) has extended this capability to wings of arbitrary planform with twist and camber. These methods, however, provide estimates of only the theoretical thrust which may or may not be attainable in the real flow.

At present, methods for estimating the fraction of the thrusting force actually attainable (e.g., ref. 4) are based on average conditions on the wing as a whole and are applicable at or near cruise conditions. Thus, the existing

methods provide no information on locally attainable thrust or on its spanwise distribution. Such information would be useful in understanding the phenomena and could lead to the development of design methods for maximization of attainable thrust and the attendant performance benefits.

This report presents a study of the factors which place limits on the thrust and describes an empirical method for estimation of attainable thrust. The method is suitable for programming as a subroutine in existing methods for estimation of the theoretical leading-edge thrust.

SYMBOLS

b	wing span
c	local wing chord
\bar{c}	mean aerodynamic chord
c_{av}	average wing chord, S/b
c_t	theoretical section thrust coefficient, $dt/dy qc$
c_t^*	attainable section thrust coefficient, $dt^*/dy qc$
C_A	axial or chord force coefficient
ΔC_A	increment of axial force coefficient due to leading-edge thrust
C_D	drag coefficient
$C_{D,0}$	drag coefficient at zero lift
C_L	lift coefficient
C_N	normal force coefficient
ΔC_N	increment of normal force coefficient due to rotation of leading-edge suction vector
C_p	pressure coefficient
$C_{p,lim}$	limiting pressure coefficient used in definition of attainable thrust
$C_{p,vac}$	vacuum pressure coefficient, $-2/\gamma M^2$
C_T	theoretical wing thrust coefficient, $\frac{2}{b} \int_0^{b/2} c_t \left(\frac{c}{c_{av}} \right) dy$
C_T^*	attainable wing thrust coefficient, $\frac{2}{b} \int_0^{b/2} c_t^* \left(\frac{c}{c_{av}} \right) dy$

k_1, k_2, k_3, k_4	constants used in airfoil section definition
K_T	fraction of theoretical thrust actually attainable, c_t^*/c_t
l	wing overall length
L/D	lift-drag ratio
M	free-stream Mach number
M_e	equivalent Mach number used in definition of K_T
q	dynamic pressure
r	leading-edge radius
R	free-stream Reynolds number based on \bar{c}
s	distance along wing leading edge
S	wing area
t	theoretical section leading-edge thrust
t^*	attainable section leading-edge thrust
x, y, z	Cartesian coordinate system
α	angle of attack, radians unless otherwise specified
γ	ratio of specific heats
δ	angle between tangent to local camber surface and wing-chord plane, positive for trailing edge up, deg
η	location of maximum wing section thickness as fraction of chord
Λ_{le}	leading-edge sweep angle, deg
Λ_m	maximum-thickness-line sweep angle, deg
Λ_{te}	trailing-edge sweep angle, deg
τ	maximum wing section thickness

Subscripts:

i	= 1, 2, 3, 4, . . .
n	quantities pertaining to wing section normal to leading edge with maximum thickness at midchord (see fig. 1)

METHOD DEVELOPMENT

Development of this method for the prediction of attainable leading-edge thrust is based on the fundamental principle that such forces must result from pressures acting on a surface and limitations on the attainable pressures and the surface areas on which they act form the only restraints on the achievement of theoretical thrust. The general plan of development covers three phases. First, the relationships between streamwise airfoil sections and sections normal to the leading edge are established so that a two-dimensional analysis may be conducted. Then a program for subsonic airfoils is employed to define limitations on the theoretical thrust imposed by airfoil geometry restraints and by arbitrarily defined limiting pressures. Finally, experimental data for two-dimensional airfoils were used to evaluate the practical limiting pressures and their dependence on Mach number and Reynolds number.

Normal Airfoil Derivation

For purposes of this analysis, the familiar concepts of simple sweep theory were employed. As shown in figure 1, the free-stream flow is separated into two parts, with one component of velocity parallel to the leading edge and the other perpendicular or normal to the leading edge. It is assumed that, through the transformations to be discussed, the streamwise section pressure distribution and the leading-edge thrust characteristics can be related to the characteristics of a two-dimensional section which is normal to the leading edge and operates in a velocity field defined by the normal flow vector. To define the airfoil section normal to the leading edge at any given span station, a superimposed arrow wing is introduced. This phantom wing has the same sweep angles of the leading edge, the trailing edge, and the maximum-thickness line as does the actual wing at the same span station. Derivations of the following relationships between normal and streamwise quantities are given in the appendix.

The normal-flow Mach number is defined as

$$M_n = M \cos \Lambda_{le} \quad (1)$$

The chord of the normal section is defined so as to place the maximum thickness at midchord. This is done to reduce the number of variables which must be studied in a subsequent analysis of two-dimensional section pressure and thrust characteristics. The ratio of the normal section chord to the streamwise section chord may be expressed as

$$\frac{c_n}{c} = \frac{2\eta}{\sin \Lambda_{le} \left[(1 - \eta) \tan \Lambda_{le} + \eta \tan \Lambda_{te} \right] + \cos \Lambda_{le}} \quad (2)$$

For an unswept trailing edge, equation (2) simplifies to

$$\frac{c_n}{c} = \frac{2\eta \cos \Lambda_{1e}}{1 - \eta \sin^2 \Lambda_{1e}}$$

And for unswept leading and trailing edges, or two-dimensional sections, the equation may be further reduced to

$$\frac{c_n}{c} = 2\eta$$

The thickness-to-chord ratio of the normal section may be expressed as

$$\frac{t_n}{c_n} = \frac{t}{c} \frac{1}{2\eta \cos \Lambda_{1e}} \quad (3)$$

and the ratio of leading-edge radius to chord for the normal section is

$$\frac{r_n}{c_n} = \frac{r}{c} \frac{1}{2\eta \cos^2 \Lambda_{1e}} \quad (4)$$

The normal section thrust coefficient is related to the streamwise section thrust coefficient by

$$c_{t,n} = c_t \frac{c}{c_n} \frac{1}{\cos^2 \Lambda_{1e}} \quad (5)$$

The normal flow Reynolds number is

$$R_n = R \frac{c_n}{c} \cos \Lambda_{1e} \quad (6)$$

In regions of the wing leading edge away from the apex and away from the wing-body juncture, the preceding expressions are believed to provide a reasonable basis for two-dimensional analysis of leading-edge thrust phenomena. In those regions where the analysis is most questionable, thrust values are generally small and errors in the attainable levels should have little impact on the overall performance of the wing.

Theoretical Airfoil Analysis

For the series of symmetrical two-dimensional airfoil sections shown in figure 2, the subsonic airfoil program of reference 5 was employed to define

pressure distributions and integrated thrust coefficients. The airfoils were defined by the following equation:

$$z = k_1\sqrt{x} + k_2x + k_3x^{3/2} + k_4x^2$$

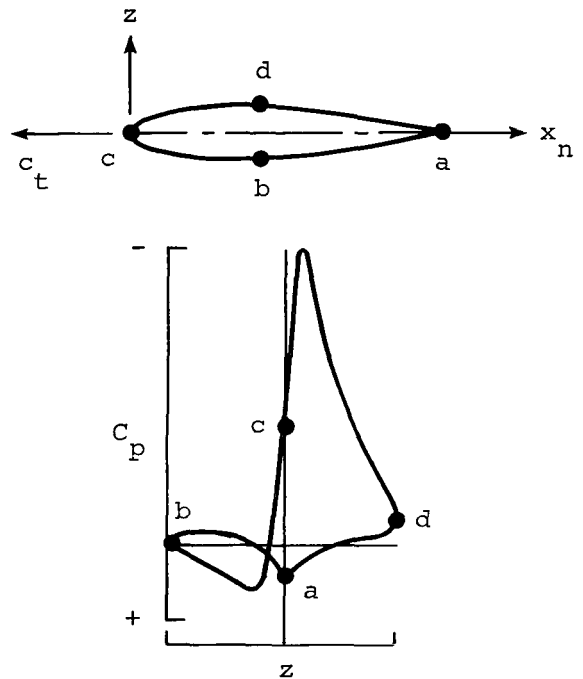
in which the coefficients were selected to produce the required chord, thickness, and leading-edge radius for a wing section with maximum thickness at mid-chord. Maximum airfoil thickness ranged from 6 percent to 18 percent of the chord, and leading-edge radius ranged from 2 percent to 16 percent of the maximum thickness. For a given airfoil, pressure distributions and thrust coefficients covering a range of normal Mach numbers were found by applying the Prandtl-Glauert rule

$$C_p\sqrt{1 - M_n^2} = \text{Constant}$$

to pressure distributions obtained at a Mach number of 0.01. This simple means of handling Mach number effects was employed for the sake of consistency with methods using linearized theory for estimating theoretical thrust. A typical pressure distribution for a large angle of attack is shown in sketch (a). Program values of the integrated section thrust coefficient

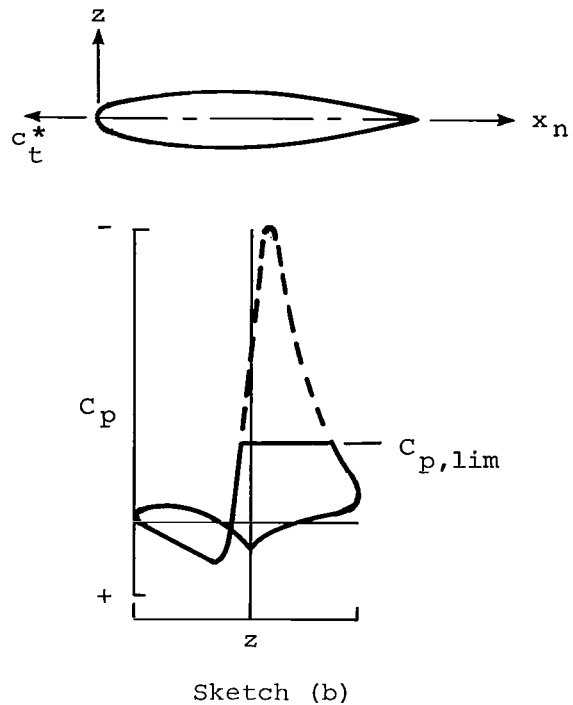
$$c_t = \frac{1}{c} \int C_p dz$$

were found to be relatively independent of the airfoil thickness and the leading-edge radius and to be in reasonably good agreement with the two-dimensional theoretical value, $2\pi\alpha^2/\sqrt{1 - M_n^2}$. The suction peak of the theoretical pressure distribution can be quite large, often exceeding the vacuum pressure limit for a given Mach number. Thus the theoretical section thrust coefficient can be unrealistically high.



Sketch (a)

In order to determine the effect on the thrust coefficient of realistically attainable pressure distributions, the program integration was performed twice: once without limitation as shown in sketch (a) and once with limitation to values greater than or equal to arbitrarily defined pressure coefficients $C_{p,lim}$ (limiting the suction peak) as shown in sketch (b). This pressure limitation is intended to account, in an approximate way, for two of the factors which limit attainable thrust: the failure to attain theoretical peak suction pressures and the tendency of these peaks to occur at a more rearward position on the airfoil. Definition of values of the effective limiting pressure coefficient will be addressed in a later section of the paper. The limited value of c_t is designated c_t^* and the attainable thrust ratio or the thrust factor is simply: $K_T = c_t^*/c_t$.



Shown in figure 3 is an example of the variation of the thrust factor with angle of attack (and with the theoretical thrust coefficient) for a given normal airfoil section at a given normal Mach number. Inset sketches show pressure distributions for 5° , 10° , 15° , and 20° angles of attack. In this example, the limiting pressure was set equal to the vacuum limit. As the figure shows, this limitation can be quite severe for large angles.

Program data are shown in figure 4 for the complete range of airfoil parameters and for normal Mach numbers of 0.3, 0.5, 0.7, and 0.9 with a limiting pressure equal to the vacuum limit. For a given normal Mach number, the thrust factor K_T was found to correlate well with the parameter

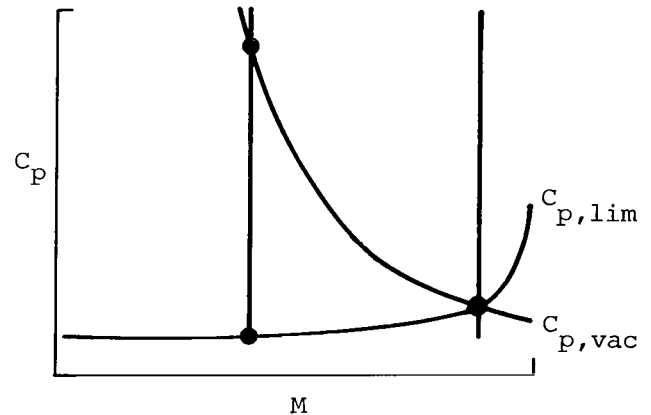
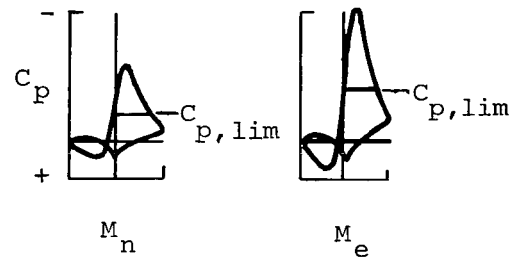
$$c_{t,n} \sqrt{1 - M_n^2} / \left(\frac{\tau_n}{c_n} \left(\frac{r_n}{c_n} \right)^{0.4} \right)$$

A thrust factor which decreases with increasing theoretical thrust is clearly shown. The correlation plot (fig. 4) also shows the tendency of increased thickness or increased leading-edge radius to improve the thrust factor. The curve fit is described by a single equation covering the full range of normal airfoil parameters and normal Mach numbers:

$$K_T = \frac{2(1 - M_n^2)}{M_n} \left[\frac{\tau_n}{c_n} \left(\frac{r_n}{c_n} \right)^{0.4} \right]^{0.6} \quad \text{but not greater than 1.0} \quad (7)$$

The limitation of K_T to values no greater than 1.0 permits attainable thrust to equal but not exceed the theoretical thrust. Note that the curve fit allows the thrust to go to zero when either the thickness or the leading-edge radius goes to zero. If both thickness and leading-edge radius go to zero, zero thrust is to be expected. However, as long as there is some thickness, an airfoil with a leading-edge radius of zero could produce a small amount of thrust because of the upper-surface suction pressure peak acting on forward facing slopes. Probably a more important consideration is that real leading-edge radii can never be zero and some attempt should be made to estimate an effective leading-edge radius for airfoils with theoretically sharp edges.

Equation (7) was developed to cover data in which the limiting pressure coefficient was set equal to the vacuum pressure coefficient. The results, however, can be generalized to cover a full range of limiting pressures between 0 and $C_{p,vac}$ for a given normal Mach number M_n by means of the following logic. As illustrated by the pressure distributions shown in sketch (c) for a given airfoil section at a given angle of attack, the pressure coefficient at any point on the airfoil will vary with Mach number according to the Prandtl-Glauert rule. If the limiting pressure $C_{p,lim}$ changes in this same fashion, the thrust factor K_T will be the same at all Mach numbers. Thus for any Mach number M_e different from the normal Mach number under consideration, K_T will be the same as for M_n provided that



Sketch (c)

$$C_{p,lim}(M_e) = C_{p,lim}(M_n) \frac{\sqrt{1 - M_n^2}}{\sqrt{1 - M_e^2}}$$

Then if M_e is selected so that $C_{p,lim}(M_e)$ is equal to the limiting vacuum pressure for that Mach number $C_{p,vac}(M_e)$, the appropriate value of K_T for the normal Mach number under consideration can be found from equation (7) by substituting M_e for M_n . The required M_e can be found by setting $C_{p,vac}(M_e)$ equal to $C_{p,lim}(M_e)$, the intersection point of the curves shown in sketch (c), and solving for M_e . Thus,

$$C_{p,vac}(M_e) = C_{p,lim}(M_e)$$

$$\frac{-2}{\gamma M_e^2} = C_{p,lim}(M_n) \frac{\sqrt{1 - M_n^2}}{\sqrt{1 - M_e^2}}$$

and on solving for the equivalent normal Mach number,

$$M_e = \frac{-\sqrt{2}}{\gamma C_{p,lim} \sqrt{1 - M_n^2}} \sqrt{1 + \left(\gamma C_{p,lim} \sqrt{1 - M_n^2} \right)^2 - 1} \quad (8)$$

Thus, the thrust factor can be expressed as

$$K_T = \frac{2(1 - M_e^2)}{M_e} \left[\frac{\frac{\tau_n}{c_n} \left(\frac{r_n}{c_n} \right)^{0.4}}{c_{t,n} \sqrt{1 - M_n^2}} \right]^{0.6} \quad \text{but not greater than 1.0} \quad (9)$$

where M_e , as defined by equation (8), covers the full range of possible limiting pressures. These expressions (eqs. (8) and (9)) describe the variation of the thrust factor with the theoretical thrust, with airfoil geometric parameters, with normal Mach number, and with limiting pressure coefficients, which will be defined in the next section.

Experimental Airfoil Analysis

In order to define practical values of the limiting pressure coefficient, the as yet incomplete prediction method was applied to experimental two-dimensional airfoil data (refs. 6 and 7) for symmetrical sections. Correlations of axial force coefficients predicted by this method with experimentally determined axial force coefficients as shown in figures 5, 6, and 7 were used to determine, by iteration, values of $C_{p,lim}$ which appeared to match the experimental trends.

Figure 5 is intended to show the leading-edge thrust behavior with changes in wing thickness for a low normal Mach number of 0.3. Although there are large changes in the fraction of theoretical leading-edge thrust actually achieved, the differences in the limiting pressure coefficient required for correlation are relatively minor, varying from 12.5 to 15.0 percent of the vacuum pressure coefficient $C_{p,vac}$ for this Mach number. In order to show the sensitivity of the limiting pressure to uncertainties in the experimental data, curves of ΔC_A as a function of α are shown in figure 5 for values of $C_{p,lim}$ 20 percent greater than and 20 percent less than the chosen value.

Shown in figure 6 are the variations in leading-edge thrust with changes in the location of maximum thickness. These data have a somewhat higher level of indicated thrust than shown in figure 5, apparently caused by the use of a tunnel-wall bleed system having a large pressure equalizing duct rather than a small one. Note the differences in the data of figures 5 and 6 for the identical NACA 64A009 airfoil section. Limiting pressure coefficients indicated by these data range from about 17 to 20 percent of the vacuum pressure coefficient.

Shown in figure 7 are the variations of attainable thrust with normal Mach number for a series of airfoil sections. In spite of some inconsistencies, there is clearly a trend of reduced leading-edge thrust coefficients and reduced limiting pressure coefficients required for correlation as the Mach number increases. This study revealed a need for better and more complete two-dimensional airfoil data for symmetrical sections. In particular, a greater range of angle of attack and a greater range of Reynolds numbers would be desirable.

A summary of the data used in defining the limiting pressure coefficient is shown in figure 8. The ratio of the limiting pressure to the vacuum pressure is shown as a function of the normal Mach number. There is obviously a strong dependence of the limiting pressure coefficient on the normal Mach number. Although the absolute value of the pressure coefficient decreases with increasing Mach number, the fraction of the vacuum pressure increases to values approaching 1.0 for Mach numbers near 1.0. There is also a weak but definite tendency of the limiting pressure coefficient to increase with increasing normal Reynolds number. The curve fit shown on figure 8 is intended to cover the Mach number and Reynolds number trends of the data. The curve fit is defined by the equation

$$C_{p,lim} = \frac{-2}{\gamma M_n^2} \left[\frac{R_n \times 10^{-6}}{R_n \times 10^{-6} + 10^{(4-3M_n)}} \right] 0.05 + 0.35(1-M_n)^2 \quad (10)$$

This form was chosen to allow the limiting pressure to approach the vacuum pressure as the Reynolds number approached infinity and to allow the limiting pressure to approach zero as the Reynolds number approached zero. With this definition of the limiting pressure, the system for estimation of attainable thrust is complete.

NOTES ON METHOD IMPLEMENTATION

The system for estimating attainable leading-edge thrust described in the preceding section of this report is intended for use as a subroutine in lifting-surface programs which provide estimates of theoretical leading-edge thrust. The following discussion covers program additions required to supply information needed in implementation of the system, reviews the steps in estimation of attainable thrust, describes the determination of flat-wing lift and drag coefficients with attainable thrust taken into account, and outlines the extension of the method to wings with twist and camber.

Computer Program Information Required

In order to implement the present method as a subroutine in existing computer programs, several requirements must be met. The first requirement is for additional input data describing the streamwise airfoil sections. Thickness ratio τ/c , leading-edge radius to chord ratio r/c , and position of maximum thickness η must be described as functions of span position. It is assumed that the wing-chord variation with spanwise position is already suitably described. Leading- and trailing-edge sweep angles, also, are expected to be provided or readily extracted from planform data. In addition, a Reynolds number based on the wing mean aerodynamic chord must be input.

Programming of Attainable Thrust Estimate

In this review of the steps to be taken in estimating the local attainable spanwise thrust distribution, the original numbering of the equations developed in the section "Method Development" is retained. For each of a large number of selected span stations, a normal Mach number, normal section parameters, and a normal thrust coefficient must be calculated. These are, respectively,

$$M_n = M \cos \Lambda_{1e} \tag{1}$$

$$c_n = \frac{2\eta c}{\sin \Lambda_{1e} \left[(1 - \eta) \tan \Lambda_{1e} + \eta \tan \Lambda_{te} \right] + \cos \Lambda_{1e}} \tag{2}$$

$$\frac{\tau_n}{c_n} = \frac{\tau}{c} \frac{1}{2\eta \cos \Lambda_{1e}} \tag{3}$$

$$\frac{r_n}{c_n} = \frac{r}{c} \frac{1}{2\eta \cos^2 \Lambda_{1e}} \tag{4}$$

$$c_{t,n} = c_t \frac{c}{c_n} \frac{1}{\cos^2 \Lambda_{1e}} \tag{5}$$

In addition, a normal Reynolds number and a limiting pressure coefficient corresponding to that Reynolds number and the normal Mach number are required:

$$R_n = R \frac{c_n}{c} \cos \Lambda_{1e} \tag{6}$$

$$C_{p,lim} = \frac{-2}{\gamma M_n^2} \left[\frac{R_n \times 10^{-6}}{R_n \times 10^{-6} + 10^{(4-3M_n)}} \right]^{0.05+0.35(1-M_n)^2} \tag{10}$$

This then permits the calculation of an equivalent Mach number M_e as

$$M_e = \frac{-\sqrt{2}}{\gamma C_{p,lim} \sqrt{1 - M_n^2}} \sqrt{1 + \left(\gamma C_{p,lim} \sqrt{1 - M_n^2} \right)^2 - 1} \quad (8)$$

Finally, the thrust factor and the attainable thrust coefficient may be determined as

$$K_T = \frac{2(1 - M_e^2)}{M_e} \left[\frac{\frac{\tau_n \left(\frac{r_n}{c_n} \right)^{0.4}}{c_n \left(\frac{c_n}{c_n} \right)}}{c_{t,n} \sqrt{1 - M_n^2}} \right]^{0.6} \quad \text{but not greater than 1.0} \quad (9)$$

The limitation of K_T to values no greater than 1.0 permits attainable thrust to equal but not exceed the theoretical thrust.

Lift and Drag for a Flat Wing

The integration of leading-edge thrust forces to obtain wing lift and drag coefficients may be handled so as to be compatible with the Polhamus leading-edge suction analogy (ref. 8). As shown in figure 9, the leading-edge suction vector is $c_t / \cos \Lambda_{le}$. In the Polhamus analogy which assumes that no leading-edge thrust is developed, this vector is assumed to rotate to a position perpendicular to the wing surface and contribute to normal force rather than axial force. The rotated vector represents the effect of a fully developed separated leading-edge vortex system. In the present method where leading-edge thrust is partially developed, it would seem logical to consider a partial rotation of the vector. In this analysis, the vector is assumed to rotate only enough to give a chord-plane component equal to the predicted attainable suction, $c_t^* / \cos \Lambda_{le}$. The component of the rotated vector perpendicular to the chord plane is assumed to give an incremental normal force associated with a partially developed separated leading-edge vortex system. In equation form,

$$\Delta C_A = -c_t^*$$

$$\Delta C_N = \frac{c_t}{\cos \Lambda_{le}} \sin \left(\cos^{-1} \frac{c_t^*}{c_t} \right)$$

The incremental normal force vector is shown in figure 9 acting at the wing leading edge. Actually, the effect of the separated leading-edge vortex would be felt at some distance behind the leading edge. For a flat wing, the incremental normal force is not sensitive to this location, but the pitching moment

is. In this analysis, no attempt was made to define an effective location of the vector representing the separated vortex; it was assumed to act at the wing leading edge.

Extension to Wings With Twist and Camber

The present method for estimation of attainable leading-edge thrust has been developed for flat wings with symmetrical sections. However, the method should be adaptable to wings with limited twist and camber when it is coupled with lifting-surface programs capable of providing accurate theoretical leading-edge thrust distributions. Figure 10 will help to illustrate this application. Since the airfoil profile in the immediate vicinity of the leading edge has a dominant influence on the thrust characteristics, it should be possible to analyze the attainable thrust by performing calculations for a comparable symmetric wing section. This section would have a plane of symmetry which is tangent to the mean camber surface of the nonsymmetrical section at some point (perhaps the center of the leading-edge radius) near the leading edge. The superimposed symmetrical section could be assumed to have the same thickness ratio, leading-edge radius, and location of maximum thickness as the cambered section. The thrust vector would be assumed to act at an angle δ with respect to the wing-chord plane defined by the tangent to the camber surface. If the camber angle δ is small, the incremental axial and normal force coefficients can be defined as

$$\Delta C_A = -c_t \cos \left(\cos^{-1} \frac{c_t^*}{c_t} - \delta_n \right)$$

$$\Delta C_N = c_t \frac{1}{\cos \Lambda_{1e}} \sin \left(\cos^{-1} \frac{c_t^*}{c_t} - \delta_n \right)$$

where

$$\delta_n = \tan^{-1} \left(\frac{\tan \delta}{\cos \Lambda_{1e}} \right)$$

These incremental section force coefficients could then be used in a manner similar to those for the flat wing to provide estimates of twisted- and cambered-wing aerodynamic performance for realistically attainable levels of leading-edge thrust.

As for the flat wing, the incremental force normal to the lifting surface associated with a detached vortex system is assumed to act at the wing leading edge; whereas, it may actually be felt well aft of the leading edge. For a wing with twist and camber, not only will the wing normal force and pitching moment vary with the assumed vector location, but an additional incremental axial force will also be dependent on this location. Thus, the limited camber surface assumption (small δ) is quite restrictive. It should also be noted that care

must be taken to insure that the vector rotation for a twisted and cambered wing conforms to the direction of the local lifting forces at the wing leading edge. For twisted and cambered wings, there is clearly a need for a study of the proper handling in prediction techniques of the effects of partial thrust and the partial development of a separated vortex system.

COMPARISONS WITH EXPERIMENTAL DATA

The present method for estimation of attainable thrust was tested by application to wing-body configurations with flat wings and symmetrical sections for which experimental data (ref. 9) were available. Theoretical leading-edge thrust distributions were evaluated for subsonic and supersonic speeds by means of computer programs described in references 1 and 10, respectively. The attainable thrust estimate was then obtained by input of these distributions into a special, separate computer program which implemented the computational process described in the section "Notes on Method Implementation." In computing the lift curve slope and the theoretical thrust distribution, the complete wing planform through the body was employed. This was done so that body carry-over lift would not be neglected in the calculation of total lift and in the determination of leading-edge thrust. However, after theoretical leading-edge thrust distributions were obtained, that portion of the thrust inboard of the wing-body juncture was ignored. Theoretical lift and drag coefficients were formulated so as to be compatible with the Polhamus leading-edge suction analogy as described in the section "Notes on Method Implementation."

The comparisons of theory and experiment shown in figures 11 to 16 are all of the same form. Axial force coefficient, angle of attack, drag coefficient, and lift-drag ratio are given as functions of the lift coefficient. The axial force is obviously the most sensitive indicator of the presence of leading-edge thrust and should be the primary gage of the success or failure of the estimation method. The lift-drag ratio is the single most important measure of the wing-body aerodynamic efficiency, in which leading-edge thrust plays a major role, and also is an important test for the system. In observing the lift coefficient-drag coefficient polar, the transition from full or near full thrust at low lift coefficients to smaller values of thrust at high lift coefficients is of interest. The lift curve slope is defined by the basic lifting surface program, and the degree of leading-edge thrust has only a small influence. For these correlations, no attempt was made to calculate theoretical zero-lift drag; instead, the experimental drag was used. To help assess the importance of leading-edge thrust, theoretical data are shown for the limiting conditions of zero and full theoretical thrust.

In figure 11, results for the present method are compared with experimental data for an unswept wing at a Mach number of 0.6. If the method has been properly formulated, it should work for this situation where the two-dimensional flow on which the system is based is a predominant factor. In spite of the rather thin wing section (3.0-percent thickness to chord ratio) and the very small leading-edge radius (0.045 percent of the chord), an appreciable fraction of the theoretical thrust is actually developed as the method predicts.

The remainder of the comparison figures are presented as pairs or as series in which one parameter varies as the others remain essentially constant.

In part (a) of figure 12, data are shown for a delta wing with a leading-edge sweep of 45.0° while in part (b) data are shown for a sweep angle of 63.4° . In both instances, the new method gives a good estimate of the measured aerodynamic characteristics at a Mach number of 0.25 for the 5-percent-thick wing. For the 63.4° swept wing, the prediction of lift and drag is seen to be reasonably good in spite of some error in the axial force.

The three parts of figure 13 show data for a 63.4° swept delta wing with thickness ratios of 3, 5, and 8 percent at a Mach number of 0.24 and a Reynolds number of about 5×10^6 . Except for the 8-percent-thick wing, there is no appreciable discrepancy between the experimental data and the estimate by the present method. For this sweep angle and this wing section, the normal airfoil thickness ratio is about 0.3; whereas, the largest thickness used in derivation of the thrust factors was 0.18. However, there is a reasonably good prediction of the lift-drag ratio in spite of the discrepancy between predicted and measured thrust at the higher lift coefficients.

The variation of attainable thrust with Mach number may be observed in the four parts of figure 14. The wing is a 63.4° swept delta with a 5-percent-thick section. At a Mach number of 0.24, the data are little different from that seen previously. For a Mach number of 0.6, the present method predicts a decrease in attainable thrust (compared to $M = 0.24$) which is not shown by the experimental data. Nevertheless, the lift and drag predictions are still good. At a Mach number of 0.9, the experimental data and the prediction show a decrease in attainable thrust, but this does not result in a decrease in the lift-drag ratio because of the higher lift curve slope. Because of the difficulty of predicting transonic flows, the good correlation shown here may be somewhat fortuitous. At the supersonic Mach number of 1.3, there is still evidence of some degree of leading-edge thrust. Although the thrust characteristics are well predicted, there is an appreciable difference in the lift-drag ratios. The discrepancy between the theoretical and measured lift at 0° angle of attack accounts for most of this difference.

The variation of attainable thrust with Reynolds number may be explored with the aid of figure 15. The range of Reynolds numbers covered is not as large as desired; nevertheless, Reynolds number trends are evident. Thrust levels and trends indicated by the predicted axial force coefficient agree closely with the experimental data. There are, however, some discrepancies in the lift-drag ratio comparisons. There is some evidence of partially laminar flow and reduced skin friction for data at the lower Reynolds number, particularly at the lower lift coefficients. This may explain the behavior of the experimental data.

In a further attempt to define limits of applicability, unpublished data obtained at three Mach numbers for a thick wing (NACA 0008 section) with a cranked leading edge are shown in figure 16. The data were obtained as part of the SHIPS (Subsonic/Hypersonic Irregular Planform Study) Program conducted by the

National Aeronautics and Space Administration. For the inboard portion of this wing, the normal thickness ratio is 0.5, a value much larger than any considered in derivation of the thrust factor. Since this configuration employed a non-symmetric fuselage, the angle of attack for zero lift as well as the zero lift drag used for the theory were taken from the experimental data. At the Mach number of 0.6, there is some overestimation of the thrust at the larger lift coefficients, but the lift-drag ratio estimate is still good. The prediction of thrust characteristics for a Mach number of 0.9 is rather poor, but for a Mach number of 1.2, the prediction by the present method agrees well with the experimental results.

DESIGN APPLICATIONS

Because the present method of predicting attainable leading-edge thrust takes into account the spanwise variation of airfoil section characteristics, an opportunity is afforded for design by iteration to maximize the attainable thrust and the attendant performance benefits. A simplified example of such use of the method is given in figure 17. A baseline wing-body configuration having a delta wing with aspect ratio of 4 was considered. This wing employed an NACA 0005-63 section throughout the span. The design conditions chosen were a Mach number of 0.6 and a lift coefficient of 0.26 at a wind-tunnel Reynolds number of 1.5×10^6 . As shown in the spanwise thrust distribution for the baseline configuration at the left of figure 17, that configuration is estimated to achieve about two-thirds of the theoretical thrust at design conditions. A wing such as this could not be expected to develop any appreciable thrust at the outboard span stations because of limitations imposed by the sharp tip where the chord and absolute thickness both go to zero. The dashed line shown in figure 17 indicates the beginning of thrust limitation (this curve can be found from eq. (9) by setting $K_T = 1.0$ and solving for $c_{t,n}$). Levels of theoretical thrust anywhere below this line, where K_T is uniformly equal to 1.0, are estimated to be fully realizable. Above this line, K_T is less than 1.0 and the theoretical thrust will not be fully developed.

Redesign of the wing planform in an attempt to achieve a greater leading-edge thrust first involved removal of the limitations imposed by the zero tip chord, as indicated by the beginning of limitation line. When the planform was changed to that shown in the center of figure 17, the theoretical thrust level was reduced (only because the angle of attack corresponding to the design lift coefficient was reduced), but the fraction of attainable thrust was increased to about 0.78 which resulted in an increase in attainable thrust. The increase in attainable thrust coupled with the improved lift curve slope is estimated to increase the lift-drag ratio for the design condition from about 15.0 to 16.7 provided $C_{D,0}$ remains unchanged.

A further alteration in planform as shown at the right of figure 17 failed to produce an improvement over the trapezoidal planform. This does not mean, however, that a planform with curved leading edges producing a further improvement in aerodynamic efficiency cannot be found.

Further improvement in the aerodynamic performance of the trapezoidal wing by means of a change in the spanwise thickness distribution is illustrated in

figure 18. Since theoretical thrust for the design condition is indicated to a span position of about $0.3\gamma/(b/2)$, thickness changes are required only out-board of this station. A linear increase in thickness ratio from 0.05 at the $0.3\gamma/(b/2)$ station to 0.08 at the tip station is estimated to increase the attainable thrust to about 96 percent of the full theoretical thrust. If the zero-lift drag is unaltered by this change, the lift-drag ratio for the design condition is estimated to be increased to about 19.

Application of the present method to the design of wings for supersonic cruise vehicles may also be possible. Normally thrust considerations are ignored in supersonic aerodynamic theory, and wing lifting efficiency is optimized through use of twist and camber alone (e.g., ref. 10). The resultant wing camber surfaces, however, may be too severe for incorporation into practical airplane designs. The large root chord angles and the resultant large cabin floor angles are particularly troublesome. If design by iteration using the present method could result in attainment of near theoretical leading-edge thrust over even a limited range of angle of attack or lift coefficient, the wing design lift coefficient and the resultant camber surface severity could be reduced accordingly with little or no loss in aerodynamic efficiency.

CONCLUDING REMARKS

A study has been made of the factors which place limits on the theoretical leading-edge thrust, and an empirical method for estimating attainable thrust has been developed. The method is based on the use of simple sweep theory to permit a two-dimensional analysis, the use of theoretical airfoil programs to define thrust dependence on local geometric characteristics, and the examination of experimental two-dimensional airfoil data to define limitations imposed by local Mach numbers and Reynolds numbers. The applicability of the method was demonstrated by comparisons of theoretical and experimental aerodynamic characteristics for a series of wing-body configurations. Generally, good predictions of the attainable thrust and its influence on lift and drag characteristics were obtained over a range of Mach numbers from 0.24 to 1.3.

The method is compatible with the Polhamus leading-edge suction analogy for fully detached vortex flow, when the analogy is considered to represent the limiting condition of a gradual rotation of the suction vector that occurs as leading-edge thrust is lost. An additional advantage of the method is the possibility it presents for designing wings in an iterative manner to maximize thrust and the attendant performance benefits.

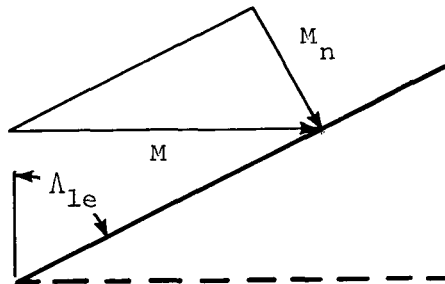
Langley Research Center
National Aeronautics and Space Administration
Hampton, VA 23665
August 24, 1979

APPENDIX

DERIVATION OF NORMAL AIRFOIL SECTION PARAMETERS

Derivation of normal airfoil sections and the appropriate flow parameters is based on simple sweep theory and on the use of a superimposed arrow-wing planform as shown in figure 1. This phantom wing has the same sweep angles for the leading edge, the trailing edge, and the maximum thickness line as does the actual wing at a given span station.

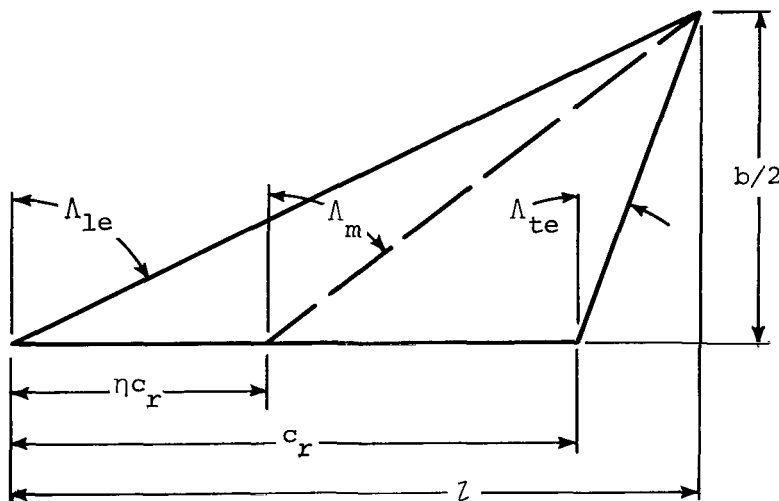
The normal Mach number is simply the component of the free-stream Mach number in a direction perpendicular to the wing leading edge, as shown in sketch (A1).



Sketch (A1)

$$M_n = M \cos \Lambda_{le} \tag{1}$$

The chord of the normal section is defined to place the maximum thickness at midchord. The sweep angle of the maximum thickness line may be obtained by consideration of the superimposed arrow-wing planform shown in sketch (A2).



Sketch (A2)

APPENDIX

$$l = \frac{c_r \tan \Lambda_{1e}}{\tan \Lambda_{1e} - \tan \Lambda_{te}}$$

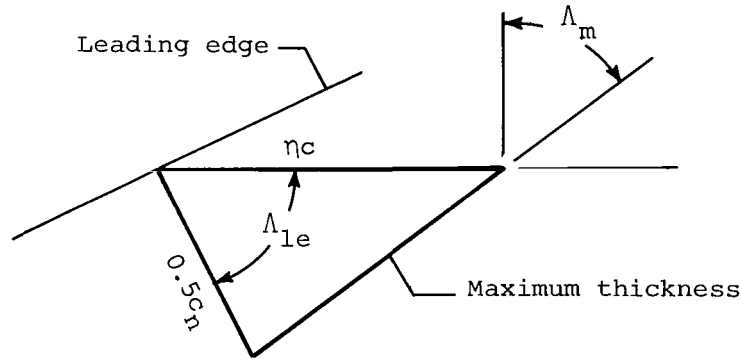
$$\frac{b}{2} = \frac{l}{\tan \Lambda_{te}}$$

$$c_r = l - \left(\frac{b}{2}\right) \tan \Lambda_{te}$$

$$\Lambda_m = \tan^{-1} \frac{l - \eta c_r}{b/2}$$

$$= \tan^{-1} \left[(1 - \eta) \tan \Lambda_{1e} + \eta \tan \Lambda_{te} \right]$$

The relationship between the normal section chord and the streamwise section chord may be established from the triangle shown in sketch (A3).



Sketch (A3)

From the law of sines,

$$\frac{0.5c_n}{\eta c} = \frac{\sin (90^\circ - \Lambda_m)}{\sin (90^\circ - \Lambda_{1e} + \Lambda_m)} = \frac{\cos \Lambda_m}{\cos (\Lambda_m - \Lambda_{1e})}$$

and

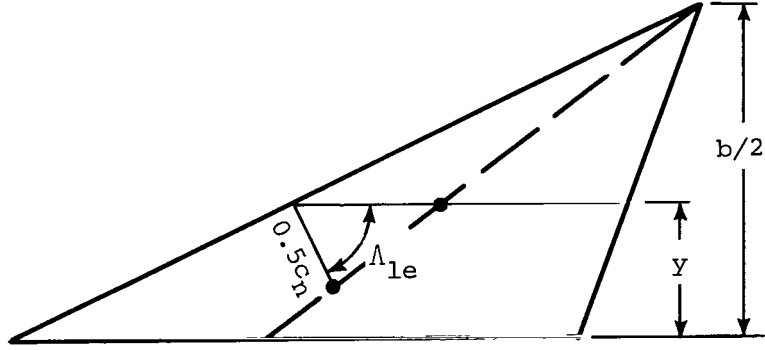
$$\frac{c_n}{c} = 2\eta \frac{\cos \Lambda_m}{\cos \Lambda_m \cos \Lambda_{1e} + \sin \Lambda_m \sin \Lambda_{1e}}$$

$$= 2\eta \frac{1}{\cos \Lambda_{1e} + \tan \Lambda_m \sin \Lambda_{1e}}$$

$$= \frac{2\eta}{\sin \Lambda_{1e} \left[(1 - \eta) \tan \Lambda_{1e} + \eta \tan \Lambda_{te} \right] + \cos \Lambda_{1e}} \quad (2)$$

APPENDIX

From sketch (A4),



Sketch (A4)

an expression for the maximum thickness of the normal section can be found:

$$\begin{aligned} \frac{\tau_n}{\tau} &= \frac{(b/2 - y) + 0.5c_n \sin \Lambda_{1e}}{(b/2 - y)} \\ &= 1 + \frac{0.5c_n \sin \Lambda_{1e}}{(b/2 - y)} \\ &= 1 + 0.5c_n \sin \Lambda_{1e} \frac{\tan \Lambda_{1e} - \tan \Lambda_{te}}{c} \end{aligned}$$

Then the normal section thickness ratio can be defined as

$$\begin{aligned} \frac{\tau_n}{c_n} &= \frac{\tau}{c_n} \left(1 + 0.5c_n \sin \Lambda_{1e} \frac{\tan \Lambda_{1e} - \tan \Lambda_{te}}{c} \right) \\ &= \frac{\tau}{c} \left[\frac{c}{c_n} + 0.5 \sin \Lambda_{1e} (\tan \Lambda_{1e} - \tan \Lambda_{te}) \right] \\ &= \frac{\tau}{c} \left\{ \frac{\sin \Lambda_{1e} [(1 - \eta) \tan \Lambda_{1e} + \eta \tan \Lambda_{te}] + \cos \Lambda_{1e}}{2\eta} \right. \\ &\quad \left. + 0.5 \sin \Lambda_{1e} (\tan \Lambda_{1e} - \tan \Lambda_{te}) \right\} \\ &= \frac{\tau}{c} \left(\frac{\sin \Lambda_{1e} \tan \Lambda_{1e} + \cos \Lambda_{1e}}{2\eta} \right) \\ &= \frac{\tau}{c} \left(\frac{\sin^2 \Lambda_{1e} + \cos^2 \Lambda_{1e}}{2\eta \cos \Lambda_{1e}} \right) \\ &= \frac{\tau}{c} \frac{1}{2\eta \cos \Lambda_{1e}} \end{aligned} \tag{3}$$

APPENDIX

A relationship between the leading-edge radius of the normal section and the leading-edge radius of the streamwise section can be derived by considering the streamwise airfoil section to be represented by the equation

$$z = k_1\sqrt{x} + \sum k_{i+1}x^{(i+1)/2}$$

in which only the first term contributes to the leading-edge radius, $r = k_1^2/2$. In the normal plane,

$$\begin{aligned} z_n &= \frac{\tau_n}{\tau} k_1 \sqrt{x_n \frac{\eta c}{0.5c_n}} + \text{higher order terms} \\ &= \frac{\tau_n}{\tau} k_1 \sqrt{\frac{\eta c}{0.5c_n}} \sqrt{x_n} + \text{higher order terms} \end{aligned}$$

with a leading-edge radius of

$$\begin{aligned} r_n &= \left(\frac{\tau_n}{\tau} k_1 \sqrt{\frac{\eta c}{0.5c_n}} \right)^2 / 2 \\ &= \left(\frac{\tau_n}{\tau} \right)^2 k_1^2 \eta \frac{c}{c_n} = \left(\frac{\tau_n}{\tau} \right)^2 2r\eta \frac{c}{c_n} \\ &= \left(\frac{\tau_n}{\tau} \right)^2 2r\eta \frac{c}{c_n} \\ &= c_n \left(\frac{\tau_n}{c_n} \right)^2 \left(\frac{c}{\tau} \right)^2 2\eta \frac{r}{c} \end{aligned}$$

Then,

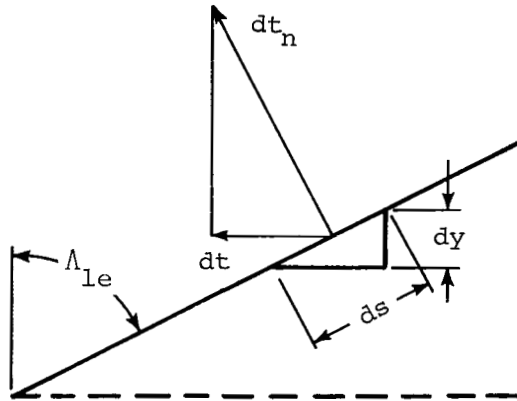
$$\begin{aligned} \frac{r_n}{c_n} &= \left(\frac{\tau_n}{c_n} \right)^2 \left(\frac{c}{\tau} \right)^2 2\eta \frac{r}{c} \\ &= \left(\frac{\tau}{c} \frac{1}{2\eta \cos \Lambda_{1e}} \right)^2 \left(\frac{c}{\tau} \right)^2 2\eta \frac{r}{c} \\ &= \frac{r}{c} \frac{1}{2\eta \cos^2 \Lambda_{1e}} \end{aligned} \tag{4}$$

APPENDIX

The section thrust coefficient may be defined as the thrusting force per unit dynamic pressure, per unit chord, and per unit spanwise distance. Thus for the streamwise section,

$$c_t = \frac{dt}{dy} \frac{1}{qc}$$

Sketch (A5) will aid in the definition of the normal section thrust coefficient.



Sketch (A5)

The thrust vector in the normal plane is

$$dt_n = \frac{dt}{\cos \Lambda_{1e}}$$

The dynamic pressure in the normal plane is

$$q_n = q \left(\frac{M_n}{M} \right)^2 = q \cos^2 \Lambda_{1e}$$

and the incremental distance in the spanwise direction for the normal section is

$$ds = \frac{dy}{\cos \Lambda_{1e}}$$

APPENDIX

The normal section thrust coefficient then becomes

$$\begin{aligned}
 c_{t,n} &= \frac{dt_n}{ds} \frac{1}{q_n c_n} \\
 &= \frac{dt}{\cos \Lambda_{1e}} \frac{\cos \Lambda_{1e}}{dy} \frac{1}{q \cos^2 \Lambda_{1e} c_n} \\
 &= \frac{dt}{dy} \frac{1}{qc} \frac{c}{c_n} \frac{1}{\cos^2 \Lambda_{1e}} \\
 &= c_t \frac{c}{c_n} \frac{1}{\cos^2 \Lambda_{1e}}
 \end{aligned} \tag{5}$$

The normal section Reynolds number differs from the streamwise Reynolds number because of changes in the velocity or Mach number and in the chord. Thus,

$$\begin{aligned}
 R_n &= R \frac{c_n}{c} \frac{M_n}{M} \\
 &= R \frac{c_n}{c} \cos \Lambda_{1e}
 \end{aligned} \tag{6}$$

REFERENCES

1. Lamar, John E.; and Gloss, Blair B.: Subsonic Aerodynamic Characteristics of Interacting Lifting Surfaces With Separated Flow Around Sharp Edges Predicted by a Vortex-Lattice Method. NASA TN D-7921, 1975.
2. Jones, Robert T.: Estimated Lift-Drag Ratios at Supersonic Speed. NACA TN 1350, 1947.
3. Carlson, Harry W.; and Mack, Robert J.: Estimation of Leading-Edge Thrust for Supersonic Wings of Arbitrary Planform. NASA TP-1270, 1978.
4. Henderson, William P.: Studies of Various Factors Affecting Drag Due to Lift at Subsonic Speeds. NASA TN D-3584, 1966.
5. Bauer, Frances; Garabedian, Paul; Korn, David; and Jameson, Antony: Supercritical Wing Sections II. Volume 108 of Lecture Notes in Economics and Mathematical Systems, Springer-Verlag, c.1975.
6. Daley, Bernard N.; and Dick, Richard S.: Effect of Thickness, Camber, and Thickness Distribution on Airfoil Characteristics at Mach Numbers up to 1.0. NACA TN 3607, 1956. (Supersedes NACA RM L52G31a.)
7. Loftin, Laurence K., Jr.: Aerodynamic Characteristics of the NACA 64-010 and 0010-1.10 40/1.051 Airfoil Sections at Mach Numbers From 0.30 to 0.85 and Reynolds Numbers From 4.0×10^6 to 8.0×10^6 . NACA TN 3244, 1954.
8. Polhamus, Edward C.: Predictions of Vortex-Lift Characteristics by a Leading-Edge Suction Analogy. J. Aircr., vol. 8, no. 4, Apr. 1971, pp. 193-199.
9. Hall, Charles F.: Lift, Drag, and Pitching Moment of Low-Aspect-Ratio Wings at Subsonic and Supersonic Speeds. NACA RM A53A30, 1953.
10. Carlson, Harry W.; and Miller, David S.: Numerical Methods for the Design and Analysis of Wings at Supersonic Speeds. NASA TN D-7713, 1974.

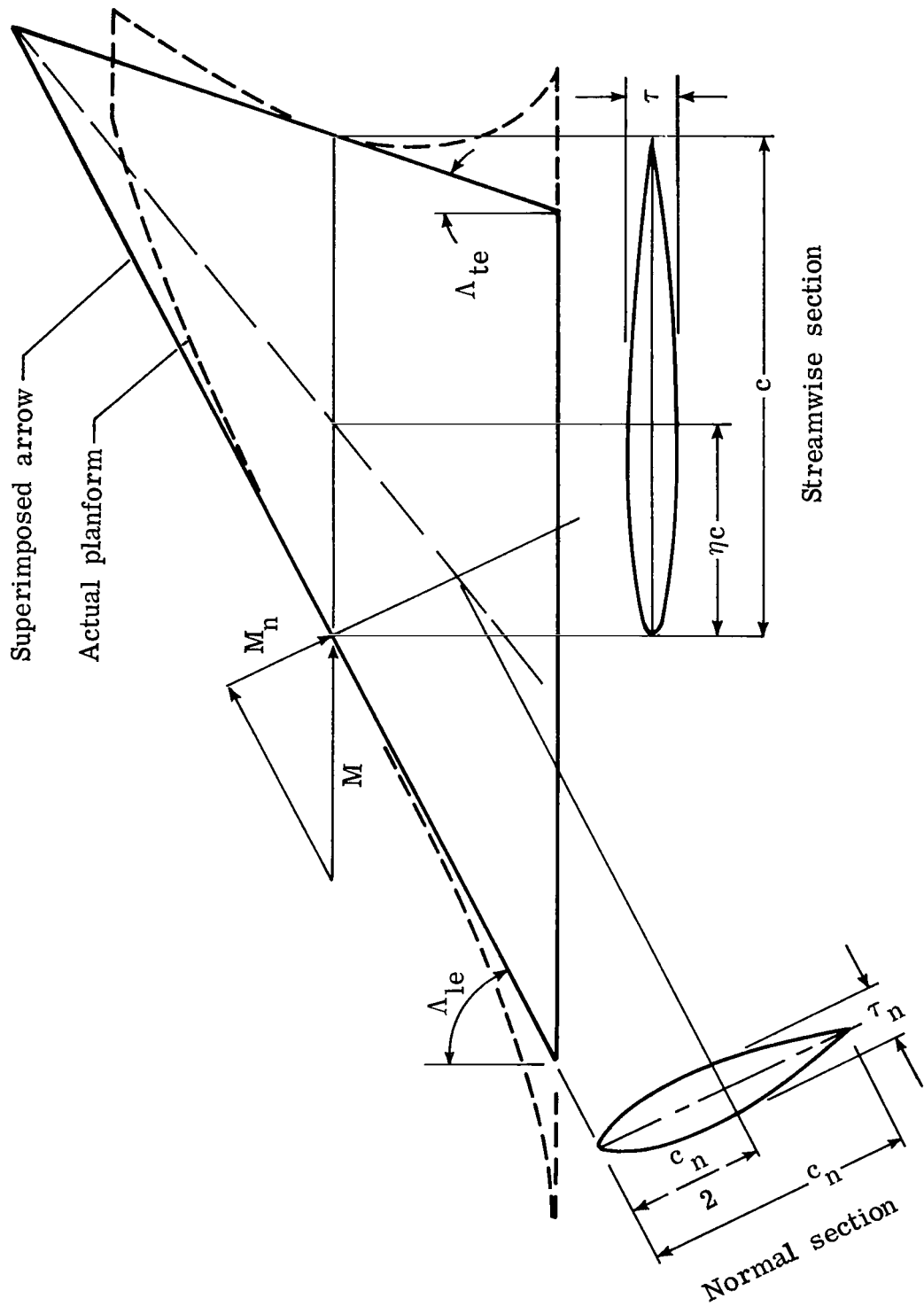


Figure 1.- Relationship between streamwise and normal wing sections.

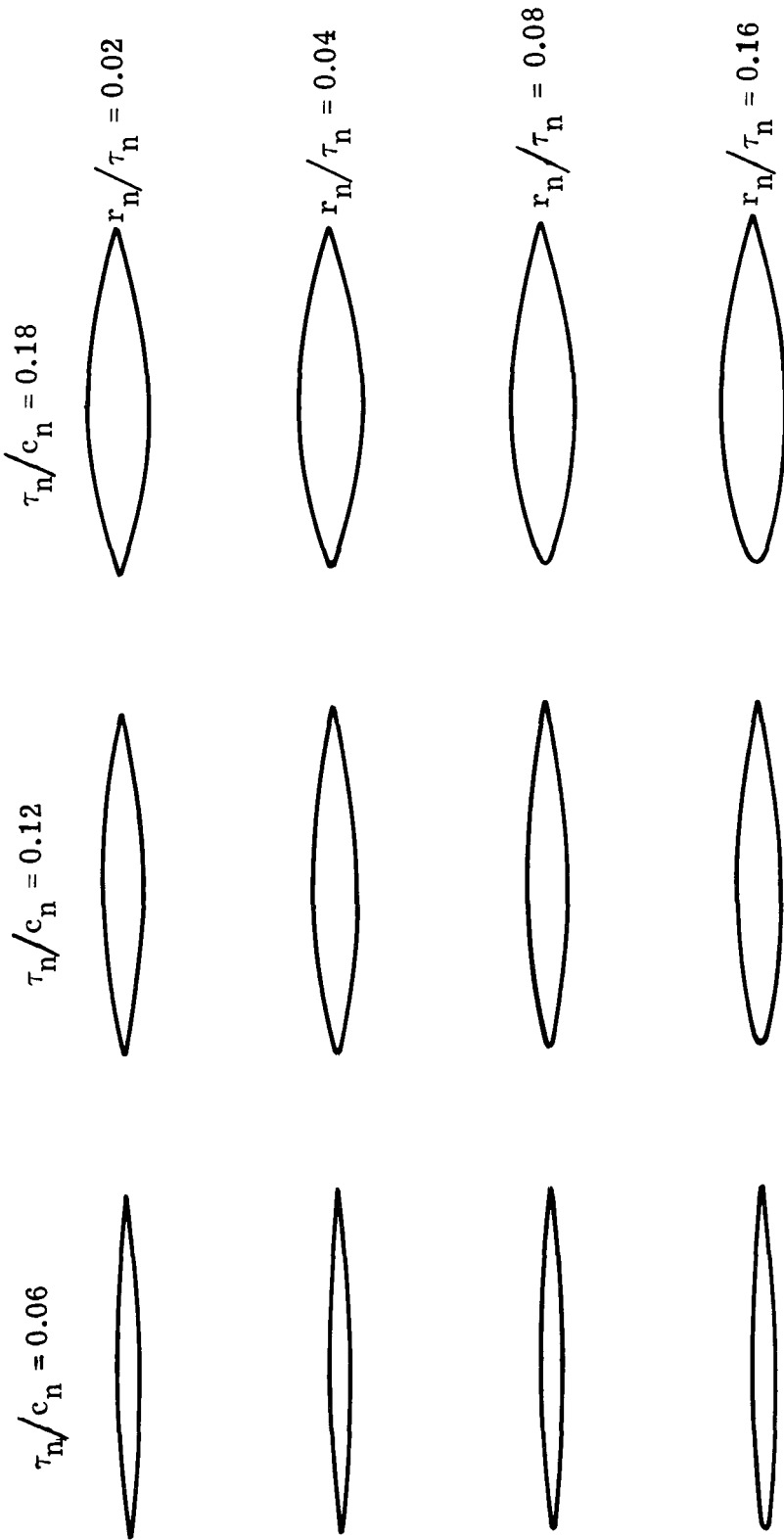
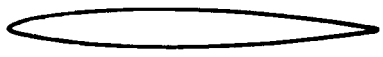


Figure 2.- Airfoils employed in analytic study.

 $\tau_n/c_n = 0.12, r_n/c_n = 0.0048$

$M_n = 0.6, C_{p,lim} = C_{p,vac} = -3.97$

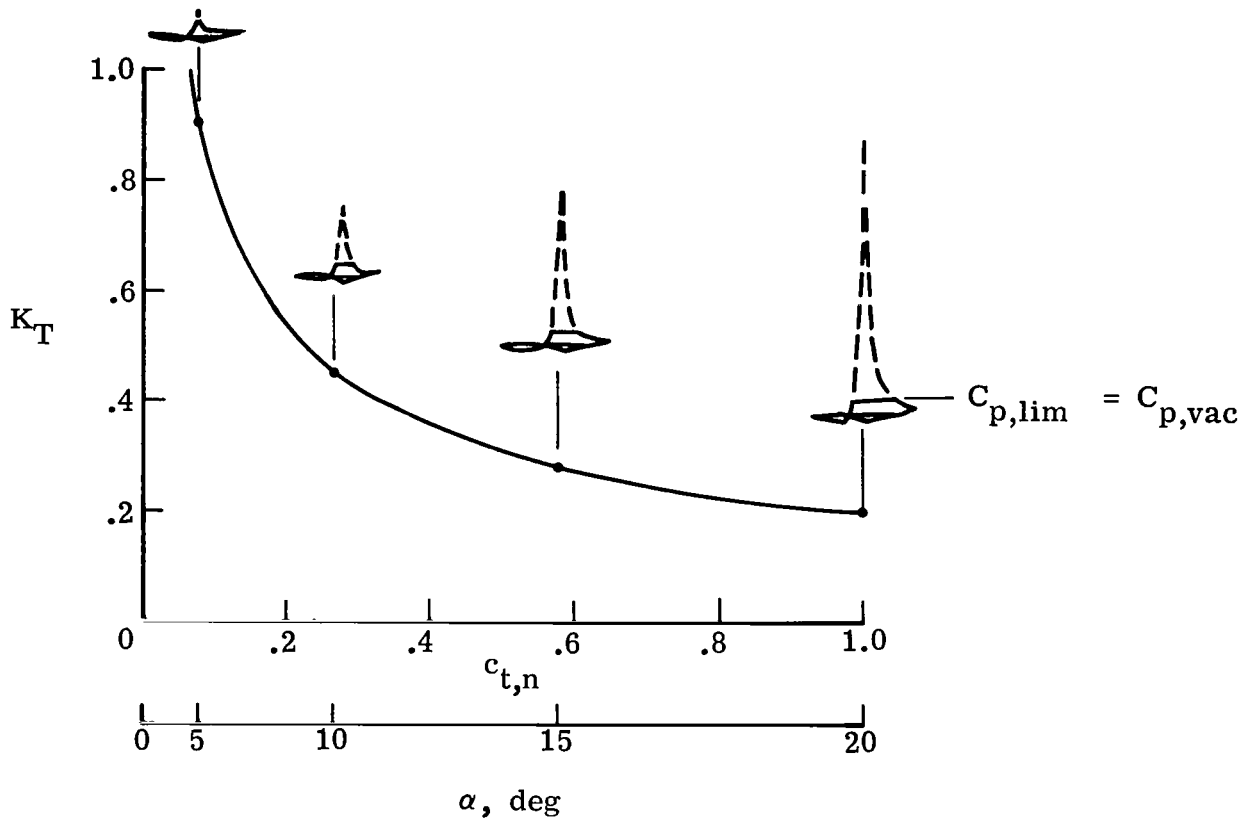


Figure 3.- Example of thrust factor variation with α and c_t for a particular airfoil.

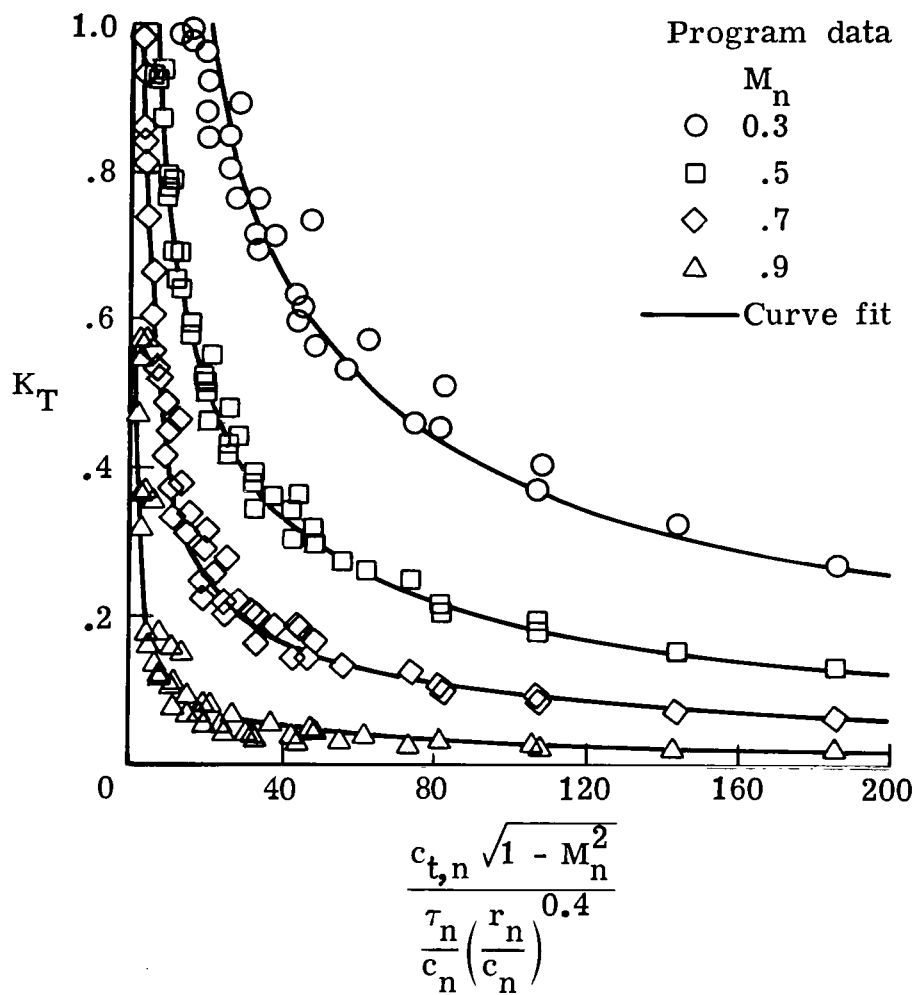


Figure 4.- Thrust factor dependence on normal airfoil parameters and normal Mach number.

○ Experiment (ref. 5), small duct

----- Theory, full thrust

———— Present method, $C_{p,lim}$ by iteration

NACA 64A004



$$\tau/c = 0.04$$

$$r/c = .0010$$

$$\eta = .39$$

NACA 64A009



$$\tau/c = 0.09$$

$$r/c = .0056$$

$$\eta = .39$$

NACA 64A012



$$\tau/c = 0.12$$

$$r/c = .0099$$

$$\eta = .39$$

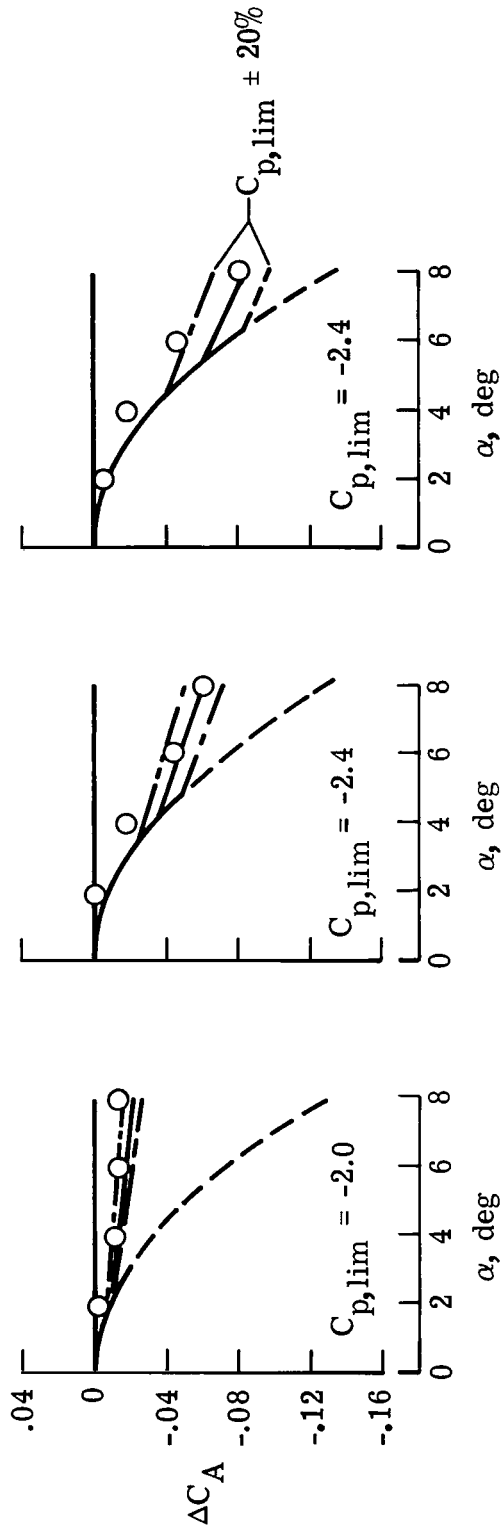


Figure 5.- Characteristics of two-dimensional airfoil for different thickness ratios; $M = 0.3$; $R = 0.67 \times 10^6$.

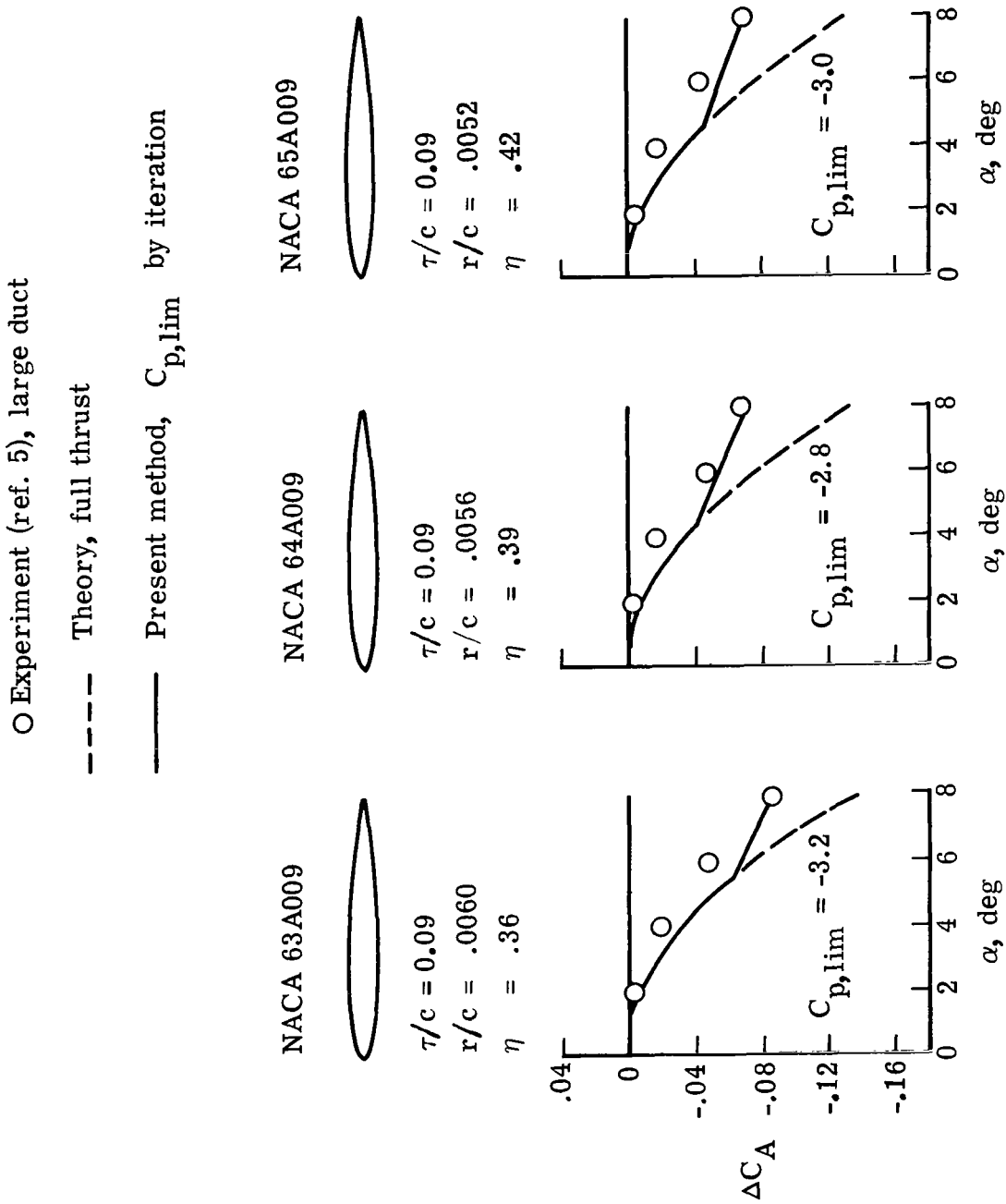
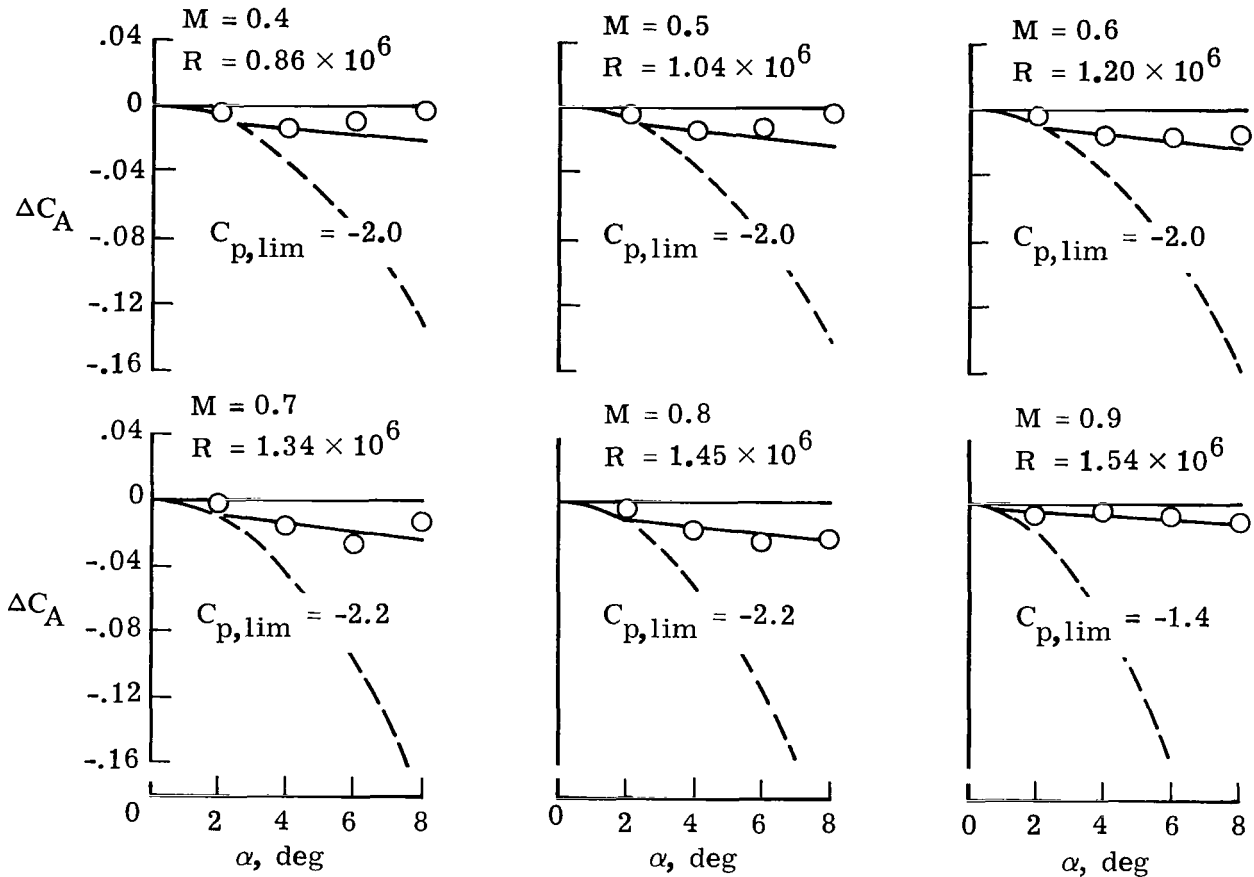


Figure 6.- Characteristics of two-dimensional airfoil for different locations of maximum thickness; $M = 0.3$; $R = 0.67 \times 10^6$.

○ Experiment (ref. 5), small duct

----- Theory, full thrust

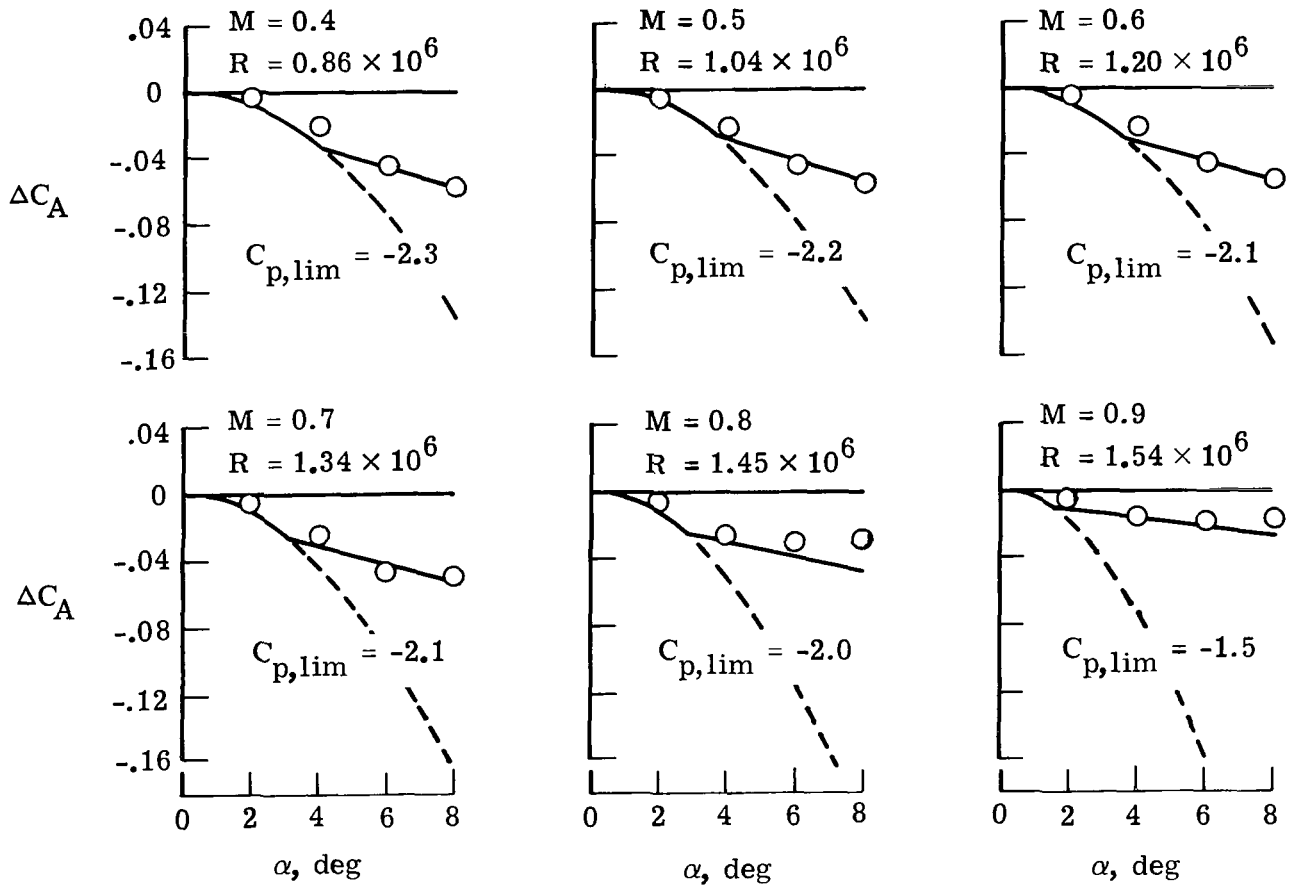
———— Present method, $C_{p,lim}$ by iteration



(a) NACA 64A004 airfoil.

Figure 7.- Characteristics of two-dimensional airfoil for different Mach numbers and Reynolds numbers.

○ Experiment (ref. 5), small duct
 - - - Theory, full thrust
 — Present method, $C_{p,lim}$ by iteration



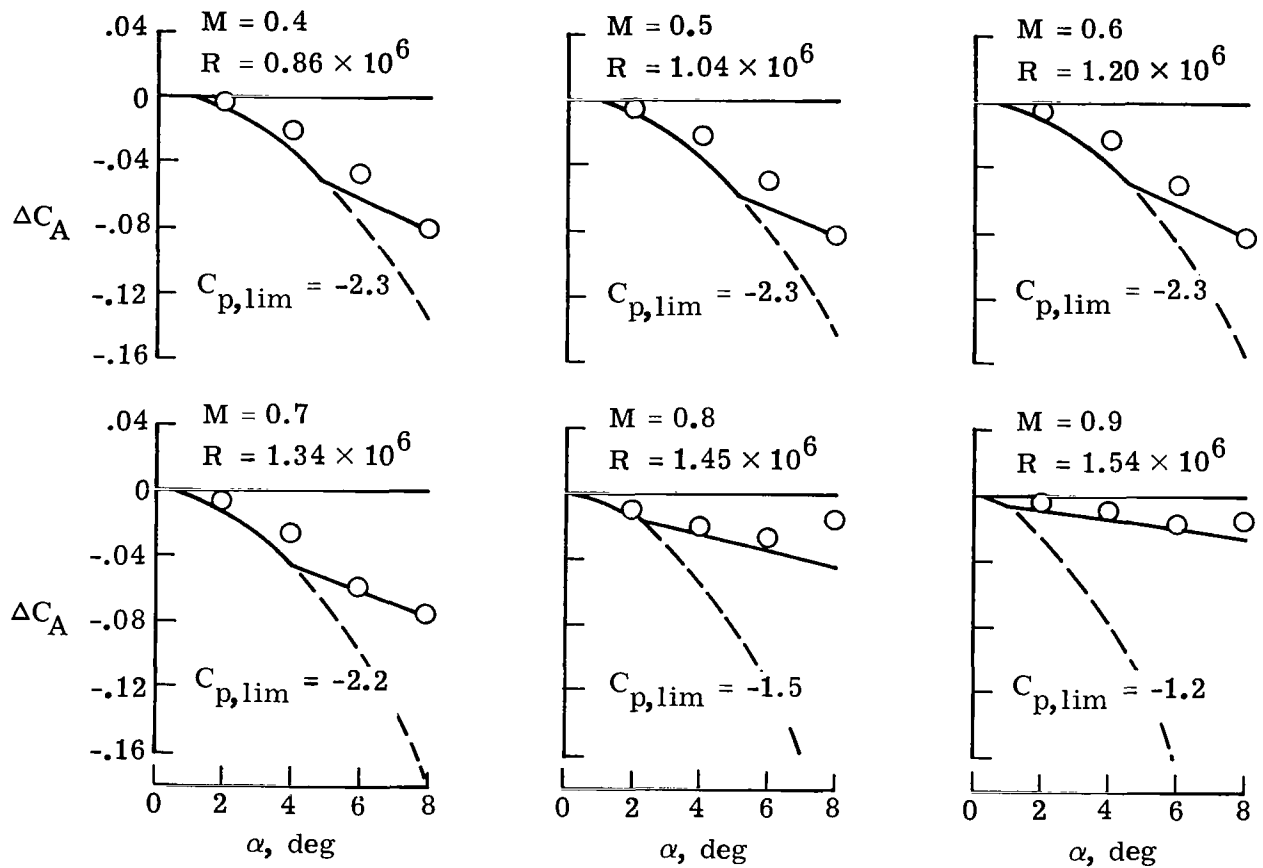
(b) NACA 64A009 airfoil.

Figure 7.- Continued.

○ Experiment (ref. 5), small duct

----- Theory, full thrust

———— Present method, $C_{p,lim}$ by iteration



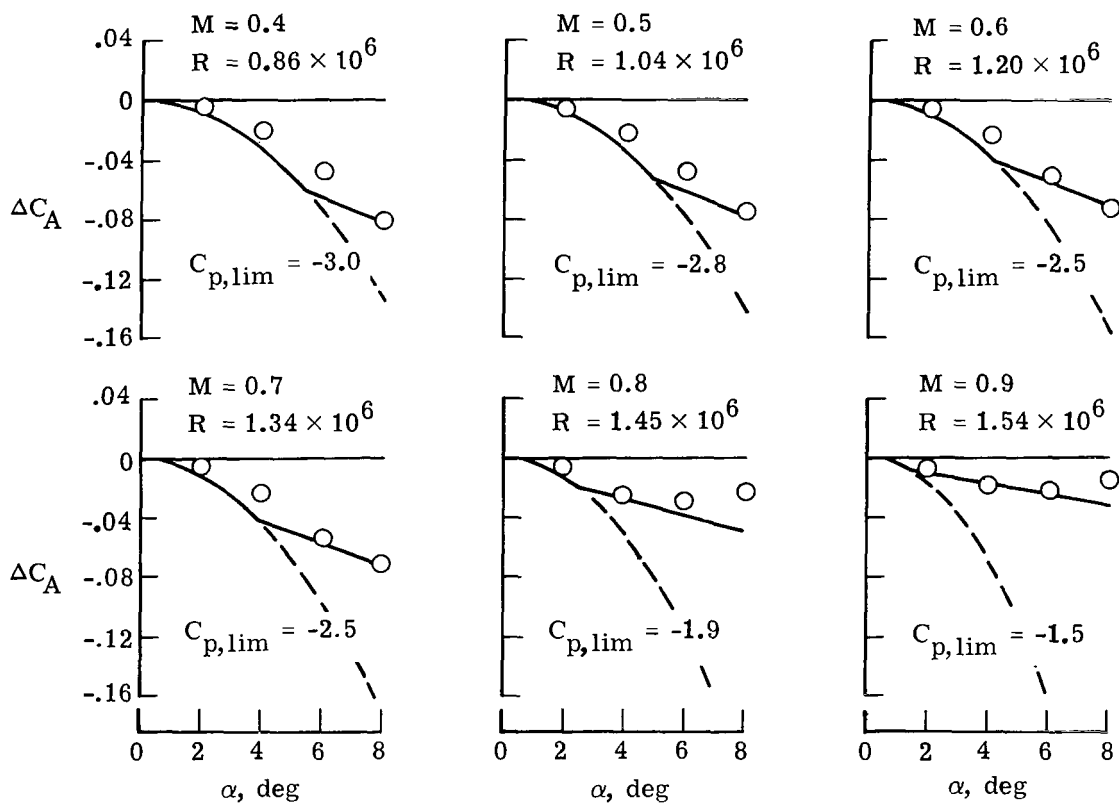
(c) NACA 64A012 airfoil.

Figure 7.- Continued.

○ Experiment (ref. 5), large duct

----- Theory, full thrust

———— Present method, $C_{p,lim}$ by iteration



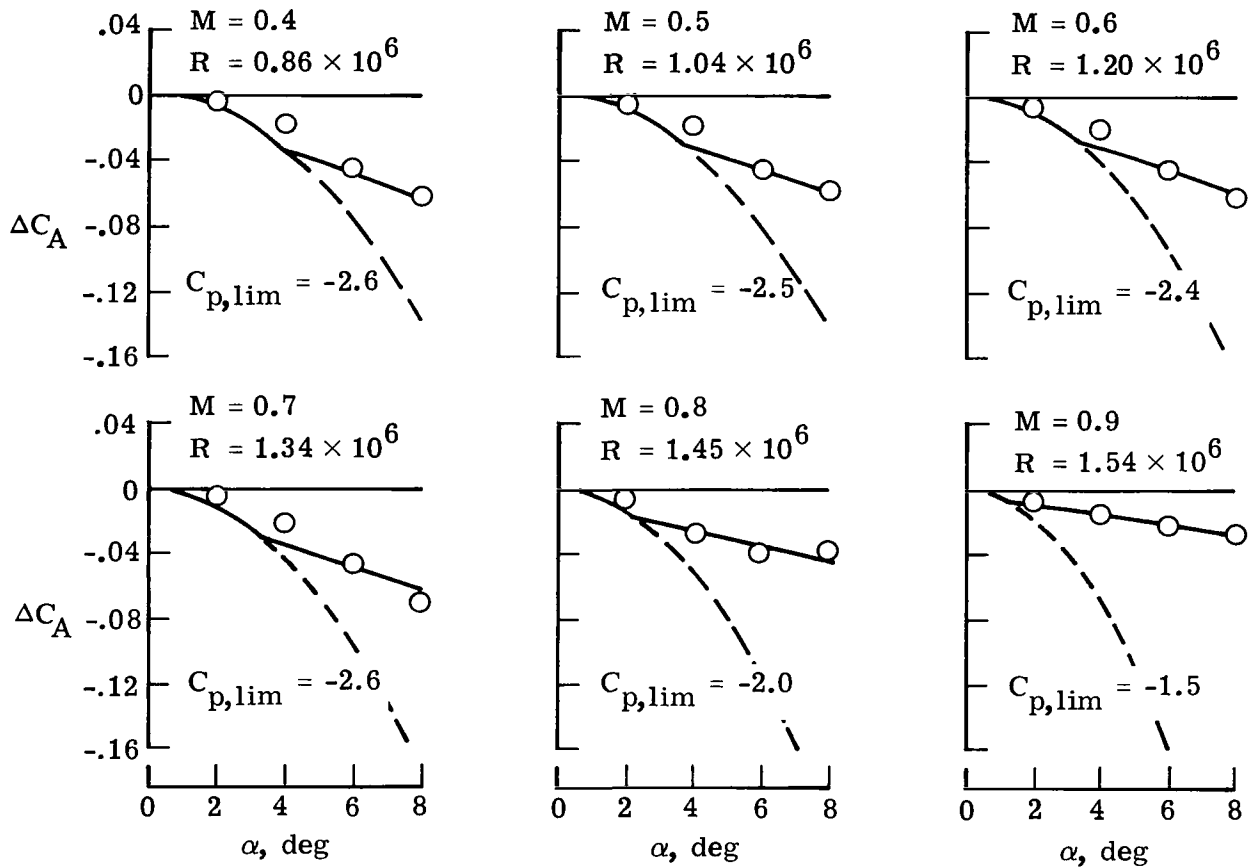
(d) NACA 63A009 airfoil.

Figure 7.- Continued.

○ Experiment (ref. 5), large duct

----- Theory, full thrust

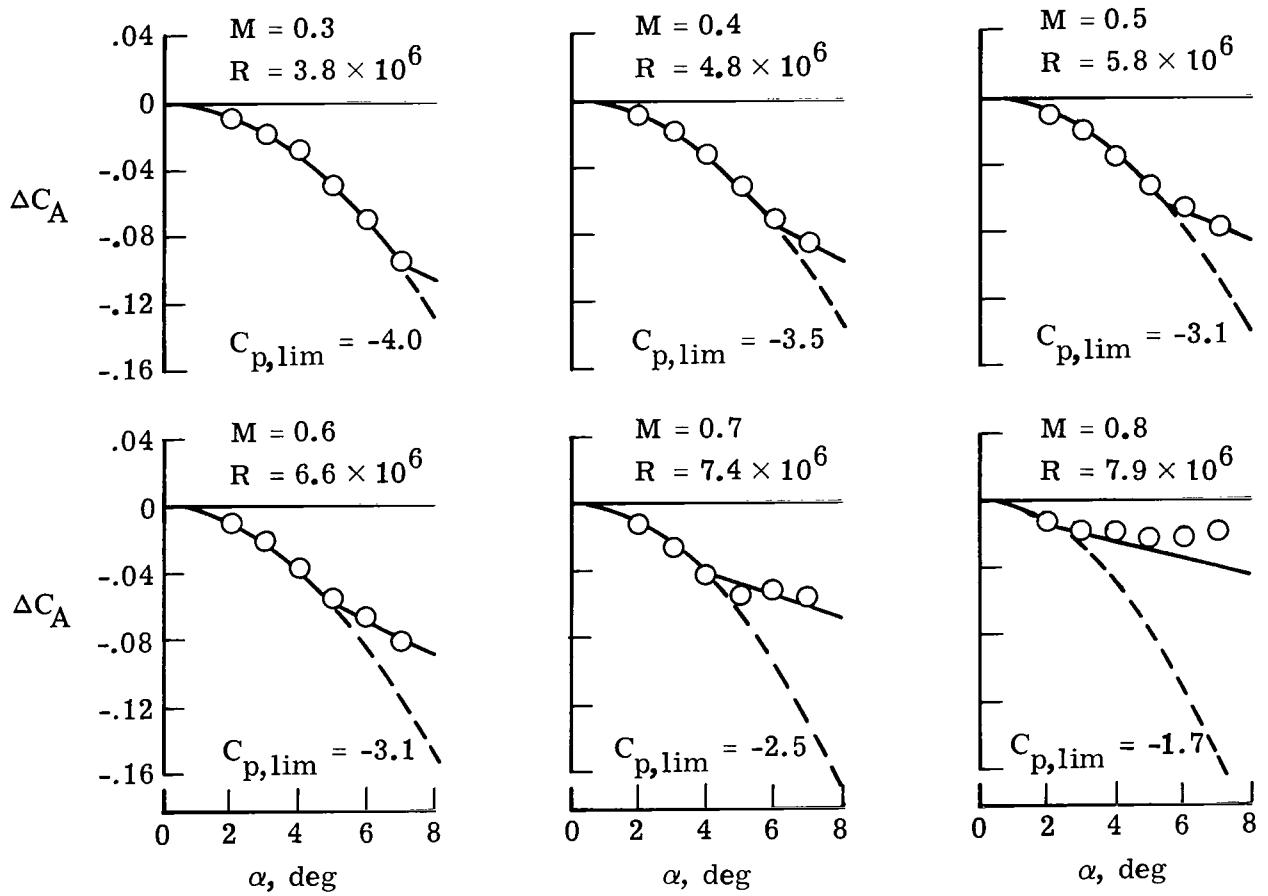
———— Present method, $C_{p,lim}$ by iteration



(e) NACA 65A009 airfoil.

Figure 7.- Continued.

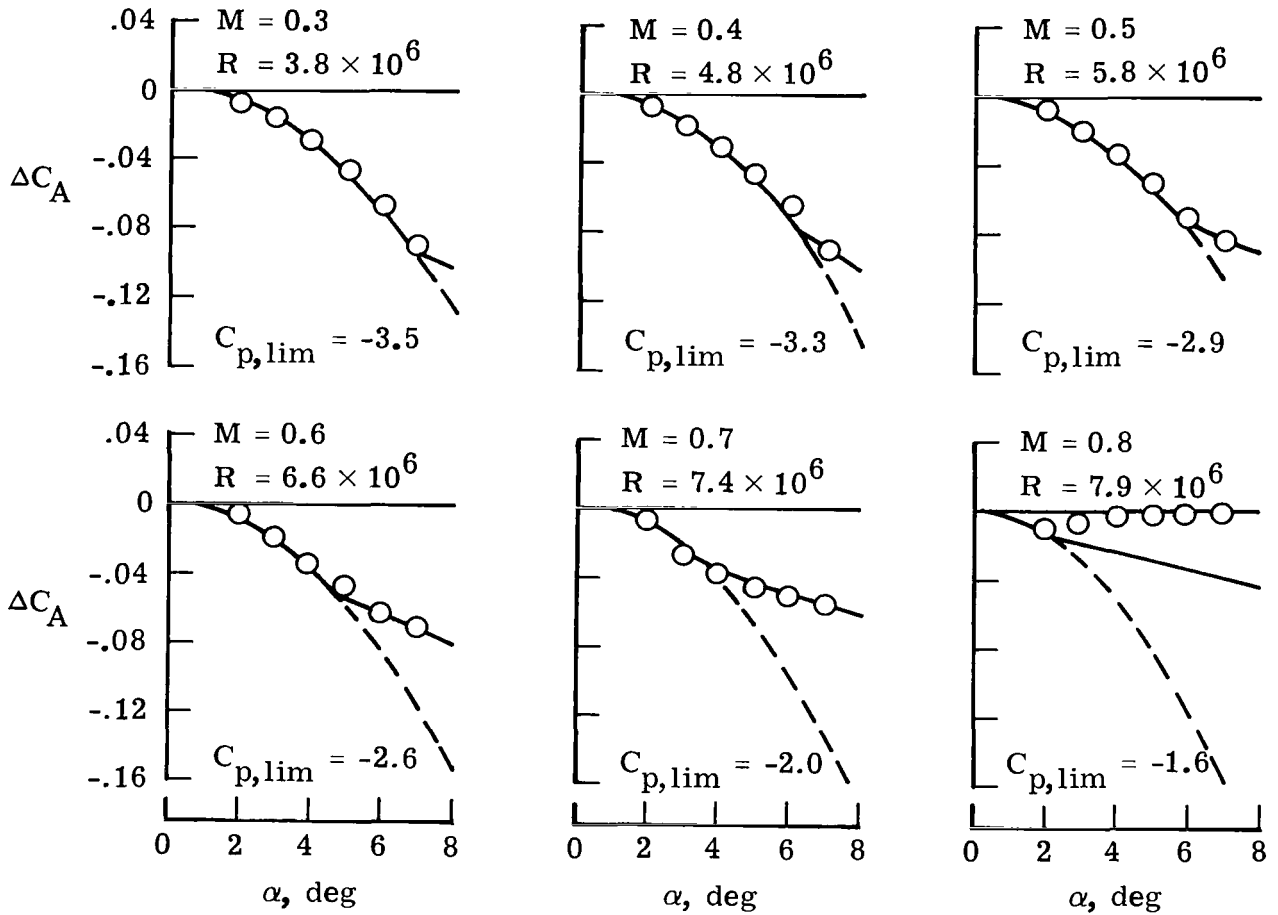
○ Experiment (ref. 6)
 - - - Theory, full thrust
 — Present method, $C_{p,lim}$ by iteration



(f) NACA 64 010 airfoil.

Figure 7.- Continued.

○ Experiment (ref. 6)
 - - - Theory, full thrust
 — Present method, $C_{p,lim}$ by iteration



(g) NACA 0010-1.10 airfoil.

Figure 7.- Concluded.

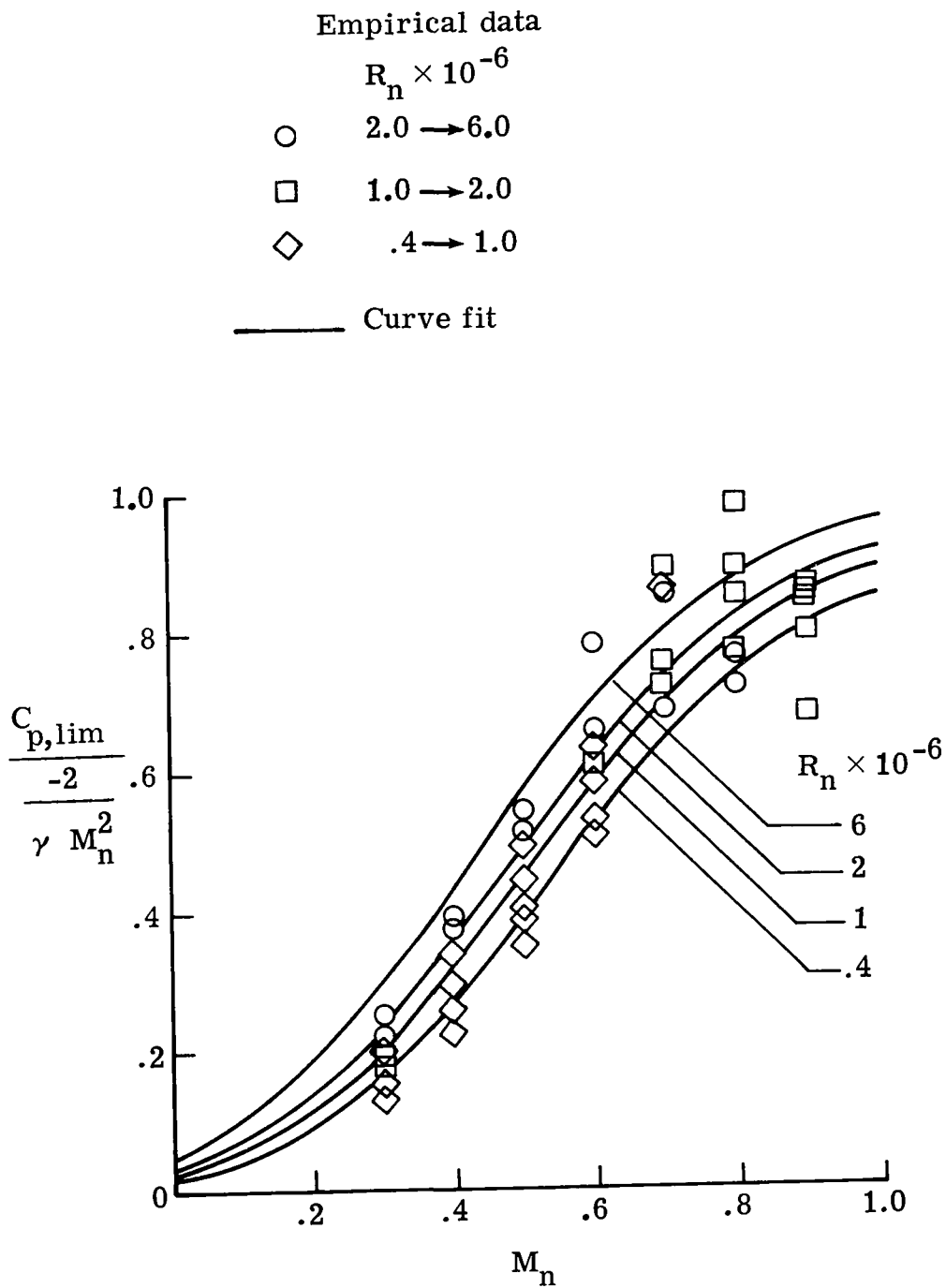


Figure 8.- Dependence of limiting pressure on normal Mach number and normal Reynolds number.

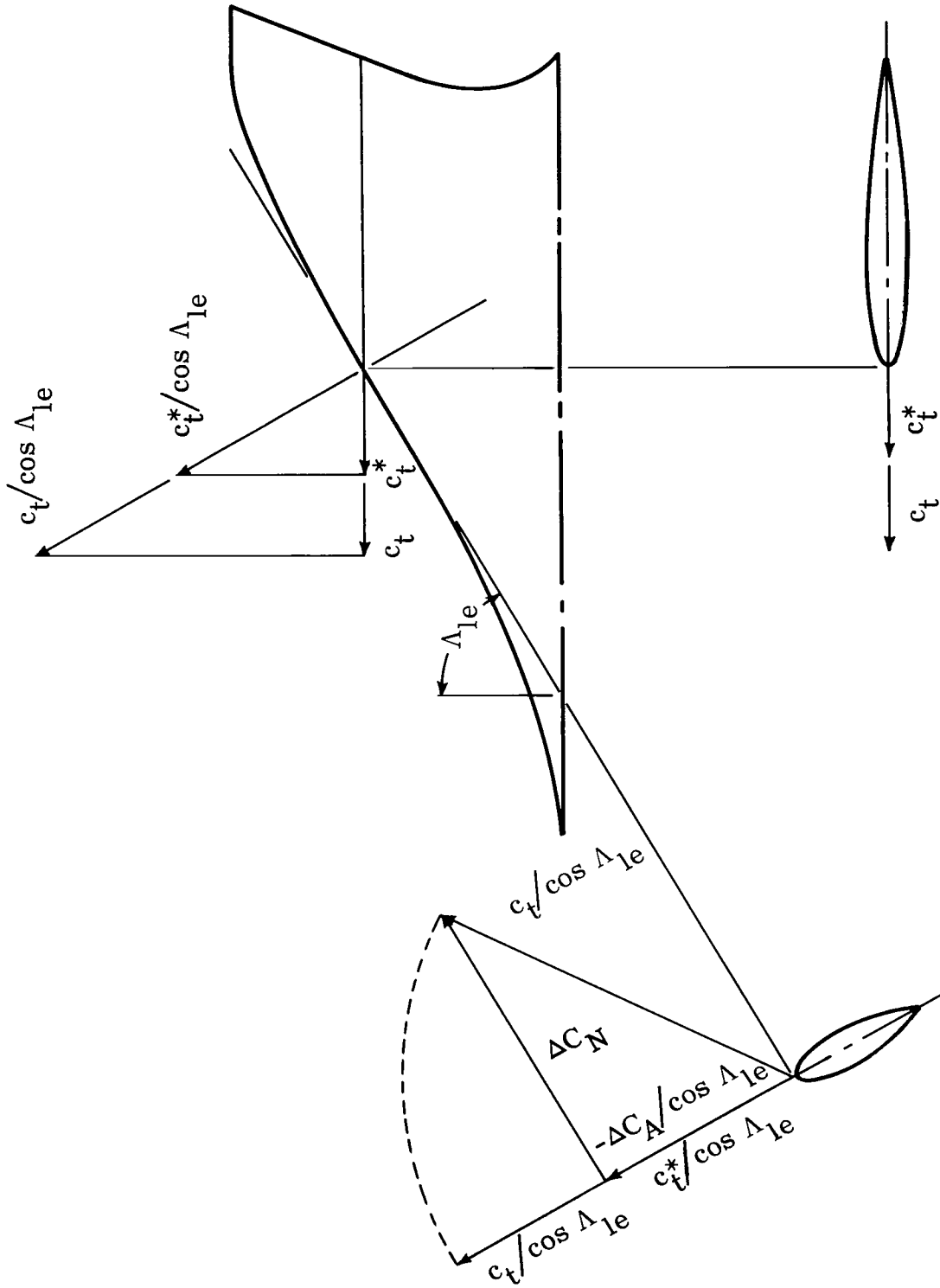


Figure 9.- Incremental section normal force associated with thrust loss for flat wing.

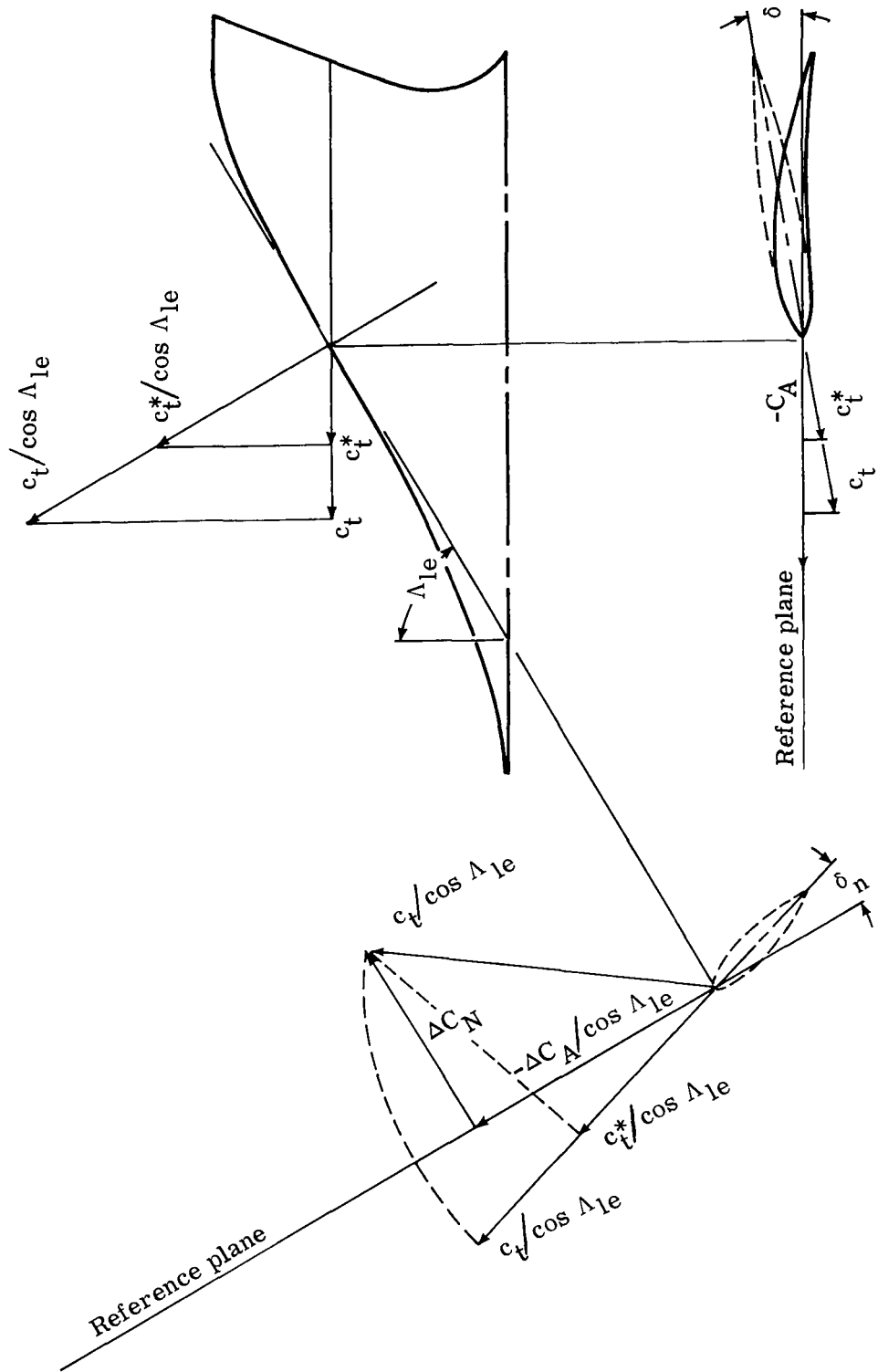
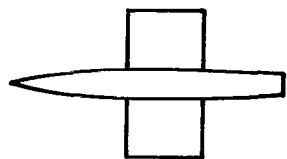


Figure 10.- Incremental section normal force associated with thrust loss for cambered wing.



3% thick
 rounded nose section
 $M = 0.61, R = 4.4 \times 10^6$

○ Experiment (ref. 8)

Theory

- No thrust
- Full thrust
- Present method

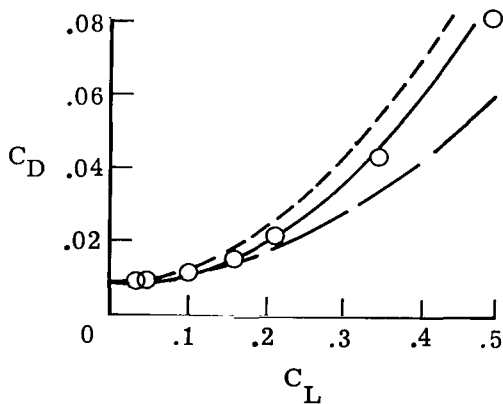
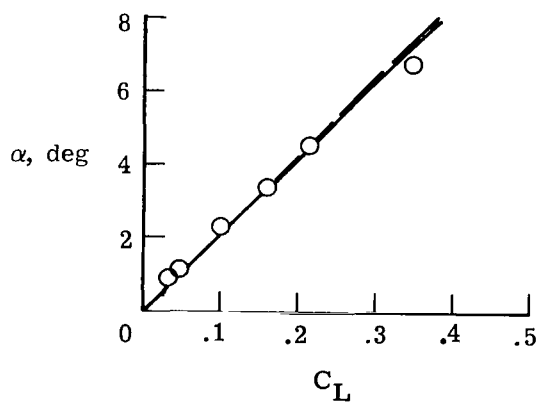
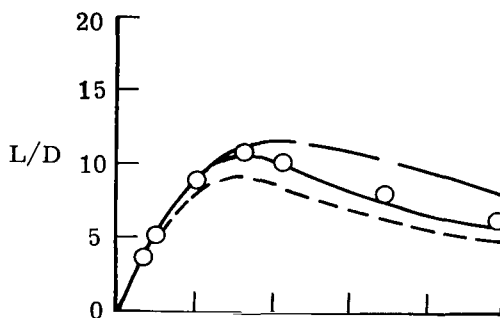
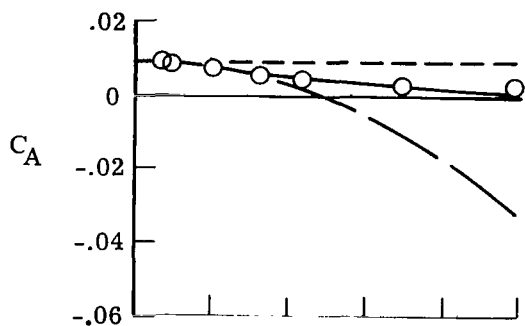
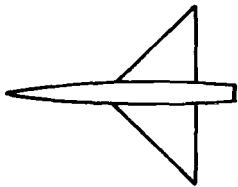


Figure 11.- Comparison of theory and experiment for unswept wing.

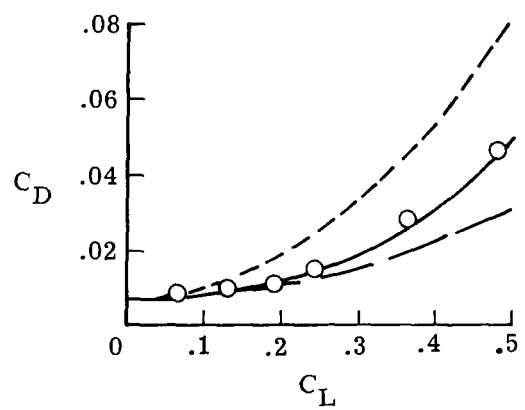
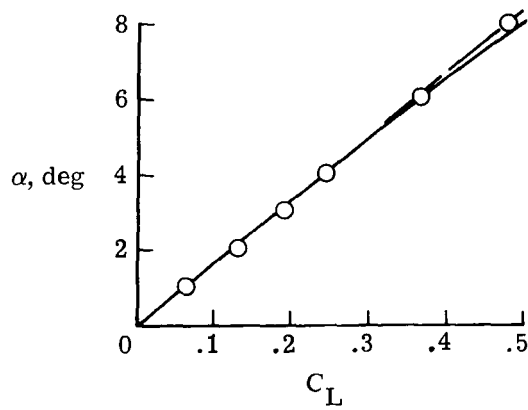
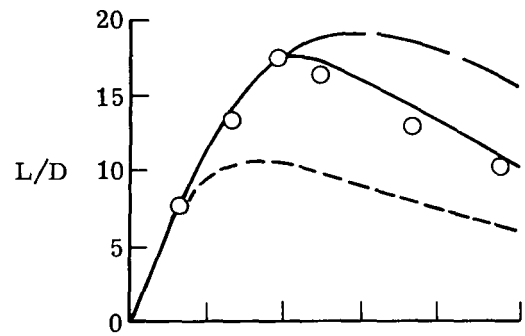
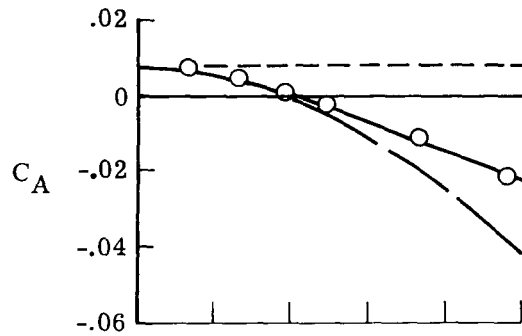


NACA 0005-63 Section
 $M = 0.25, R = 8.0 \times 10^6$

○ Experiment (ref. 8)

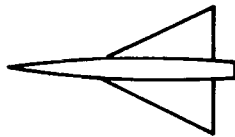
Theory

--- No thrust
 — Full thrust
 — Present method



(a) $\Lambda_{1e} = 45.0^\circ$.

Figure 12.- Comparison of theory and experiment for two leading-edge sweep angles.

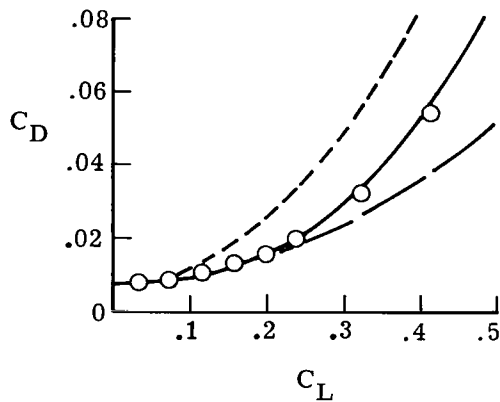
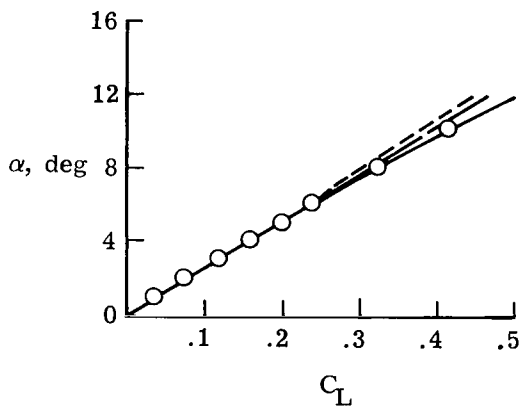
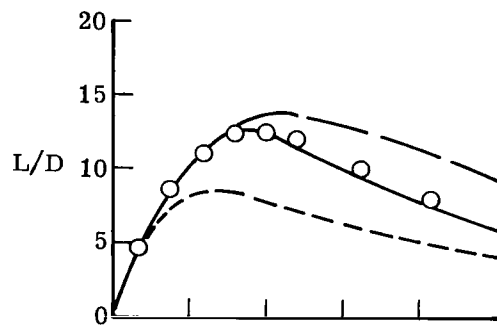
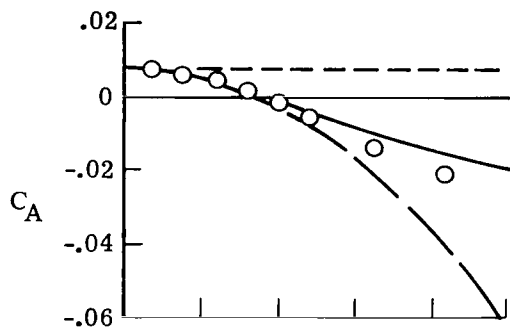


NACA 0005-63 Section
 $M = 0.25, R = 8.0 \times 10^6$

○ Experiment (ref. 8)

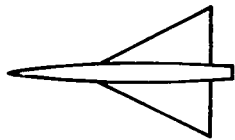
Theory

- No thrust
- Full thrust
- Present method



(b) $\Lambda_{1e} = 63.4^\circ$.

Figure 12.- Concluded.



NACA 0003-63 Section
 $M = 0.24, R = 4.9 \times 10^6$

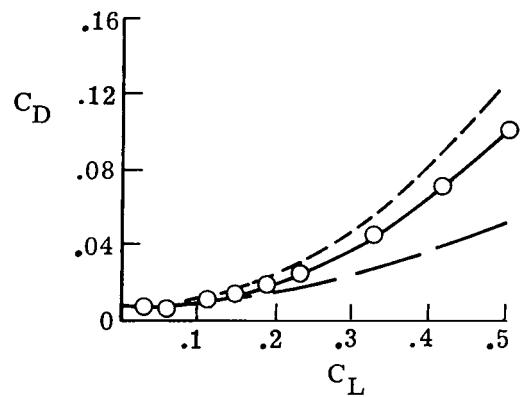
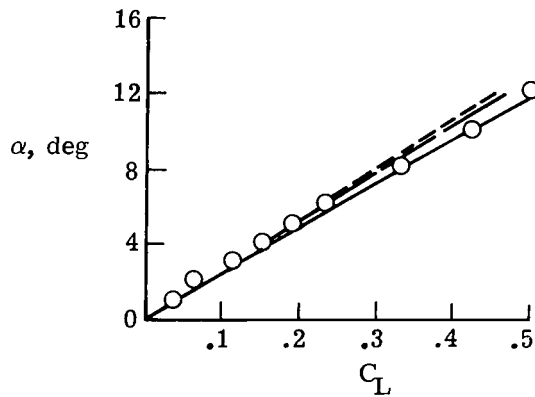
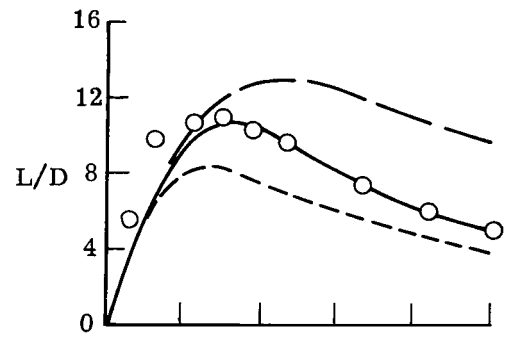
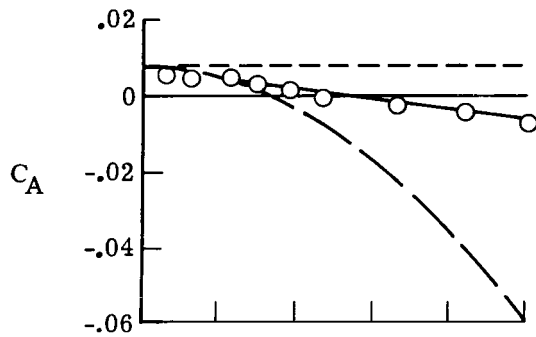
○ Experiment (ref. 8)

Theory

--- No thrust

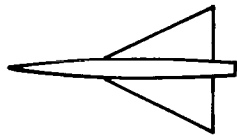
— Full thrust

— Present method



(a) 3-percent-thick airfoil.

Figure 13.- Comparison of theory and experiment for three airfoil thickness ratios; 63.4° swept delta wing.

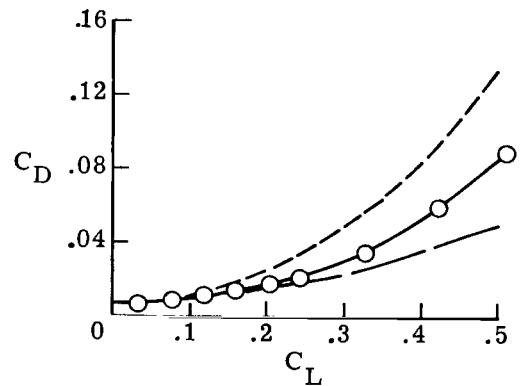
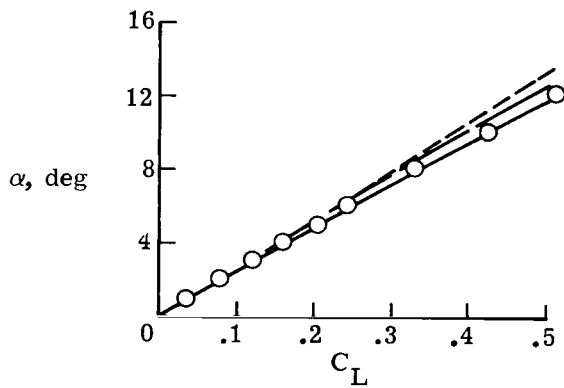
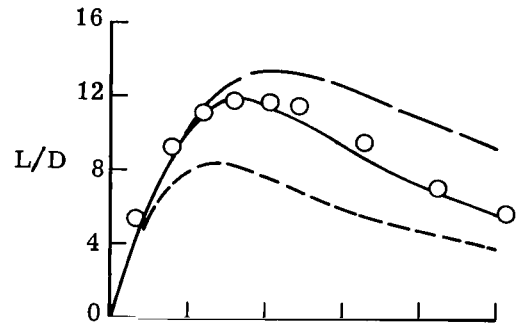
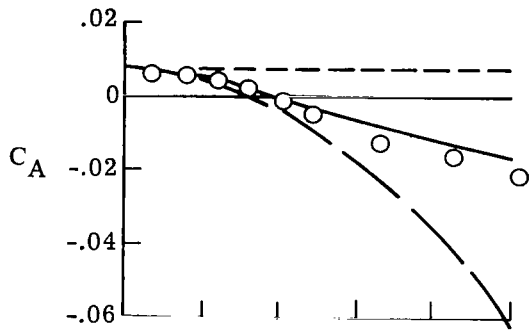


NACA 0005-63 Section 6
 $M = 0.24, R = 5.0 \times 10^6$

○ Experiment (ref. 8)

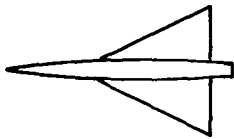
Theory

- No thrust
- Full thrust
- Present method



(b) 5-percent-thick airfoil.

Figure 13.- Continued.



NACA 0008-63 Section
 $M = 0.24, R = 5.0 \times 10^6$

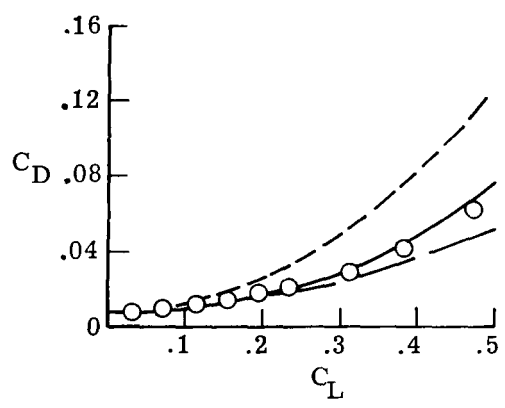
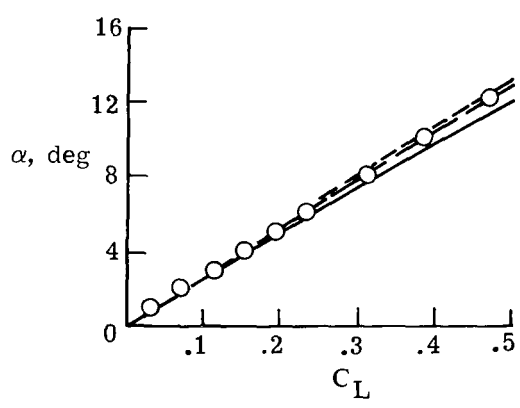
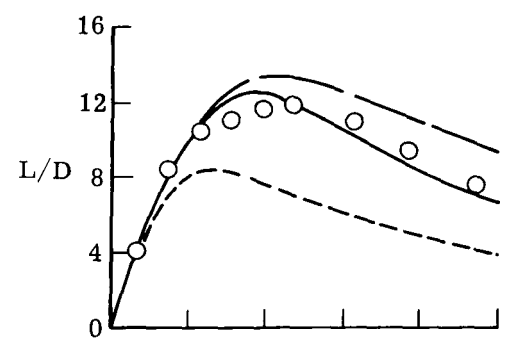
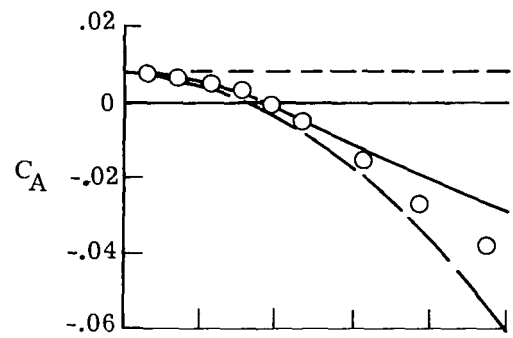
○ Experiment (ref. 8)

Theory

--- No thrust

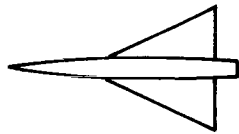
— Full thrust

— Present method



(c) 8-percent-thick airfoil.

Figure 13.- Concluded.



NACA 0005-63 Section
 $M = 0.24, R = 3.0 \times 10^6$

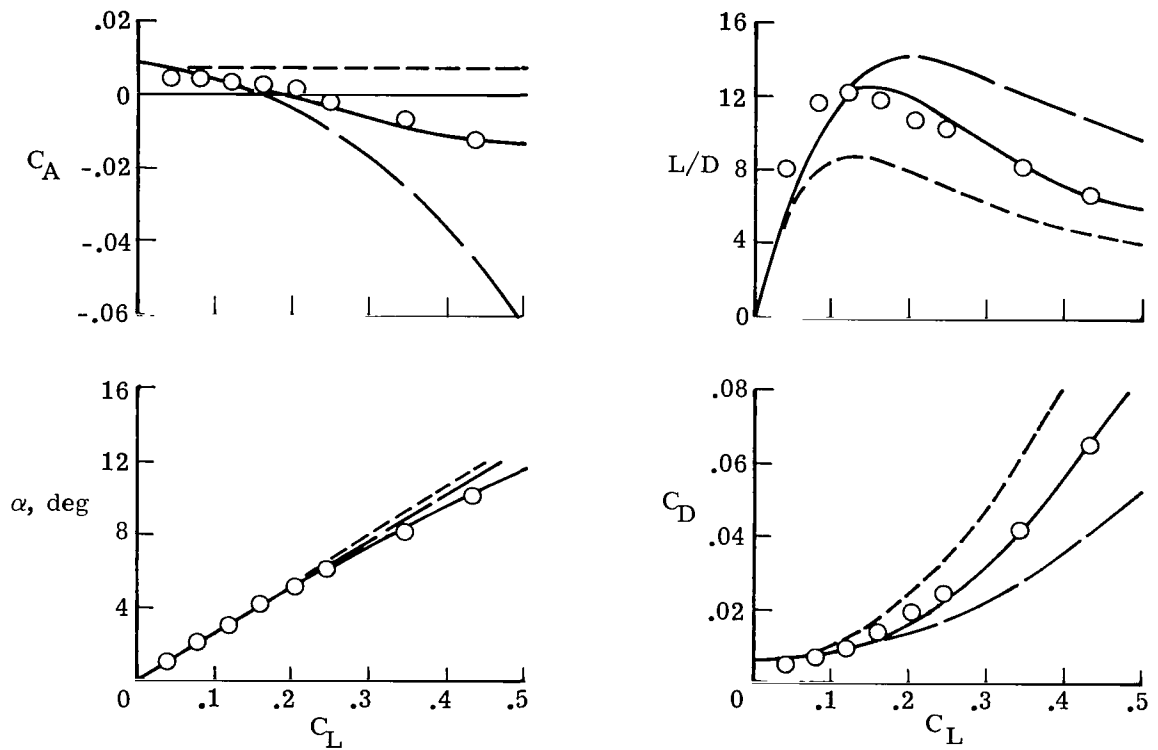
○ Experiment (ref. 8)

Theory

----- No thrust

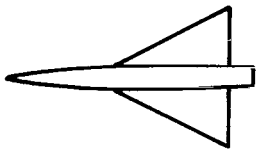
———— Full thrust

———— Present method



(a) $M = 0.24$.

Figure 14.- Comparison of theory and experiment for four Mach numbers; 63.4° swept delta wing.



NACA 0005-63 Section
 $M = 0.60, R = 3.0 \times 10^6$

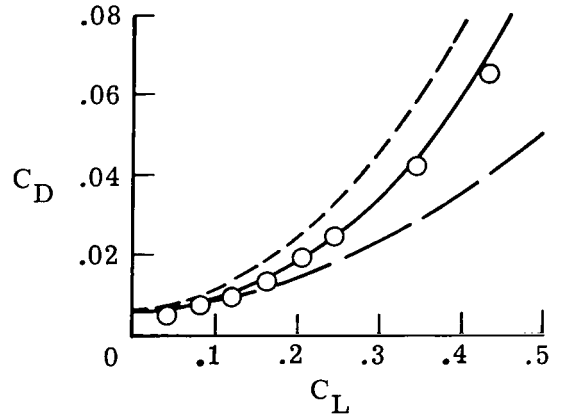
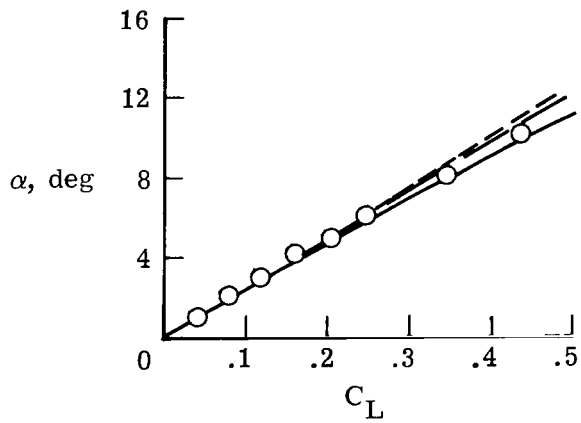
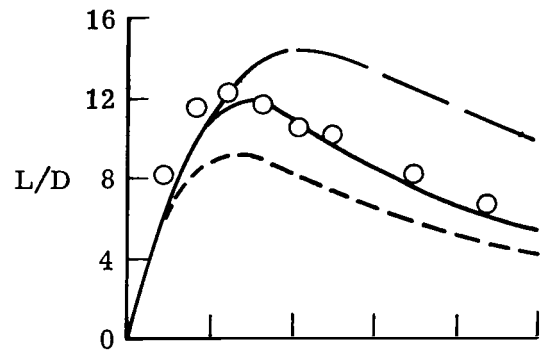
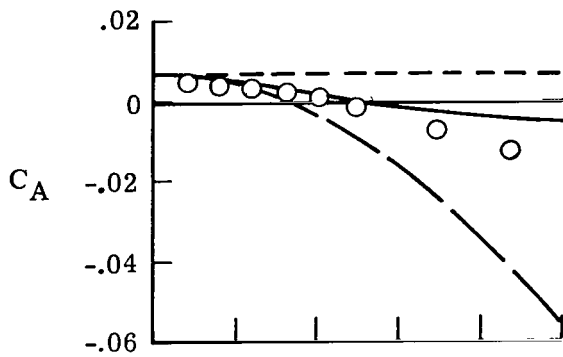
○ Experiment (ref. 8)

Theory

--- No thrust

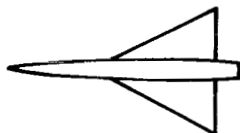
— Full thrust

— Present method



(b) $M = 0.60$.

Figure 14.- Continued.



NACA 0005-63 Section
 $M = 0.90, R = 3.0 \times 10^6$

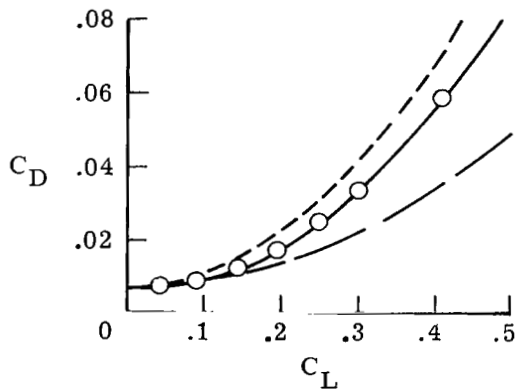
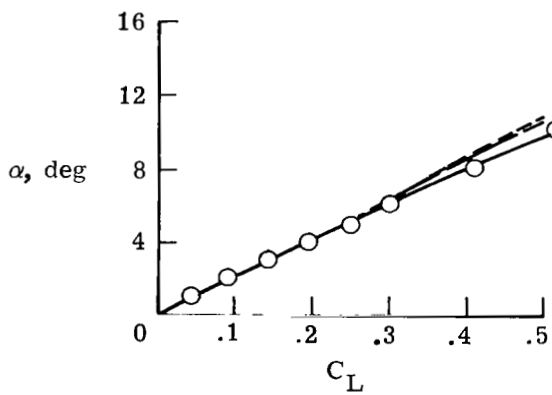
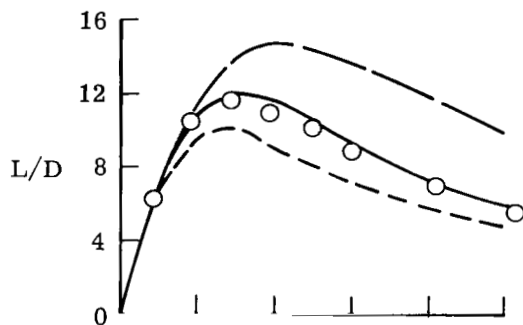
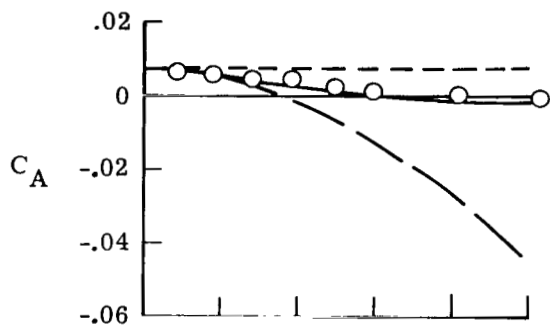
○ Experiment (ref. 8)

Theory

--- No thrust

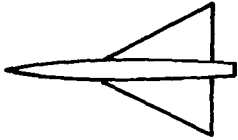
— Full thrust

— Present method



(c) $M = 0.90$.

Figure 14.- Continued.

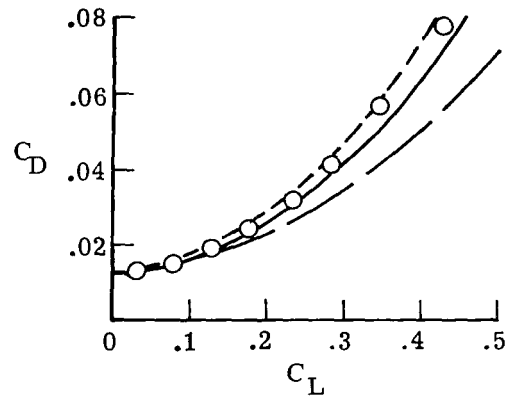
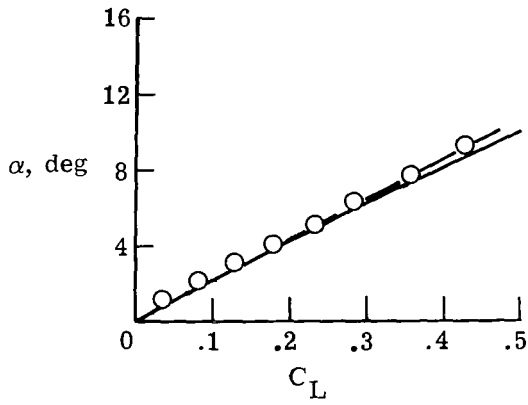
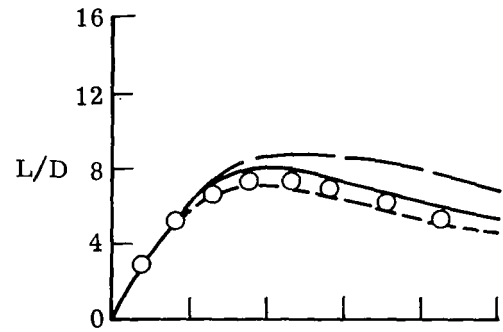
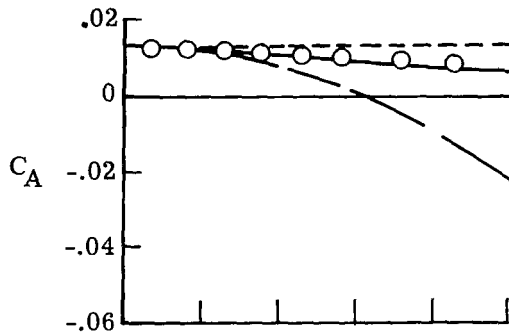


NACA 0005-63 Section
 $M = 1.3, R = 3.0 \times 10^6$

○ Experiment (ref. 8)

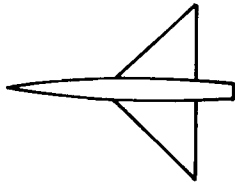
Theory

- No thrust
- Full thrust
- Present method



(d) $M = 1.3.$

Figure 14.- Concluded.

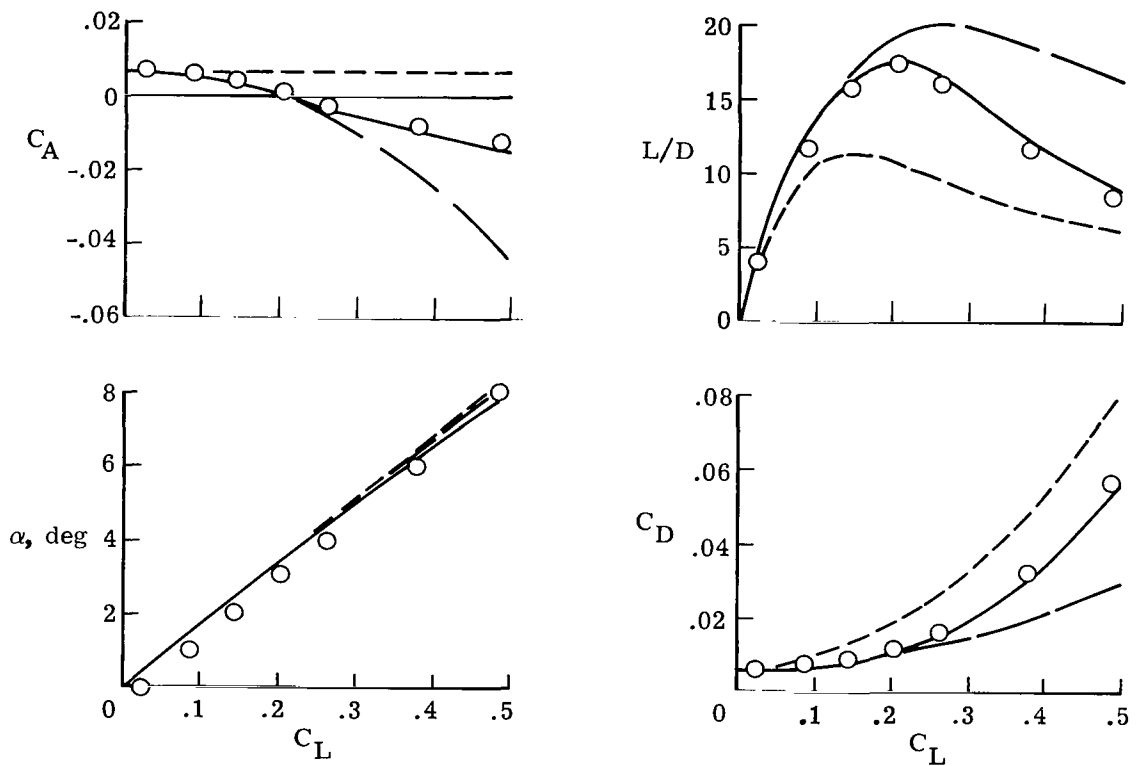


NACA 0005-63 Section
 $M = 0.25$, $R = 1.5 \times 10^6$

○ Experiment (ref. 8)

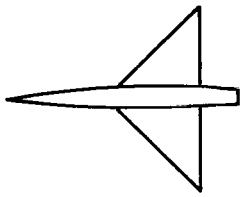
Theory

- No thrust
- Full thrust
- Present method



(a) $R = 1.5 \times 10^6$.

Figure 15.- Comparison of theory and experiment for four Reynolds numbers; 45° swept delta wing.

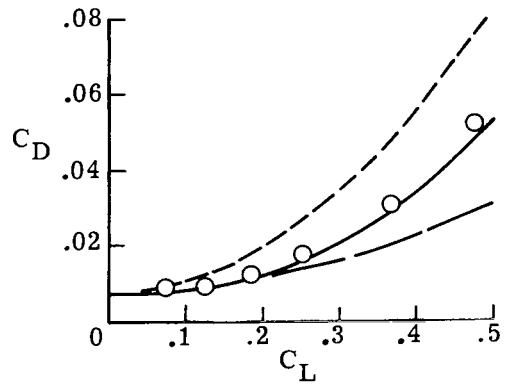
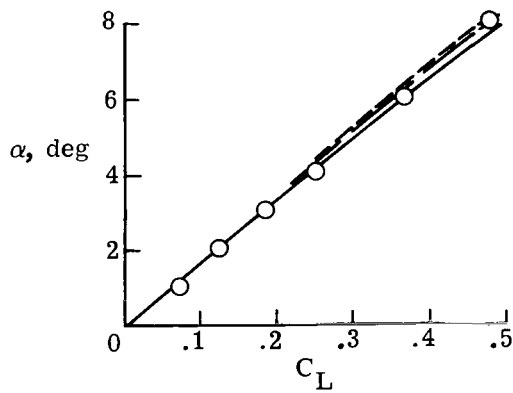
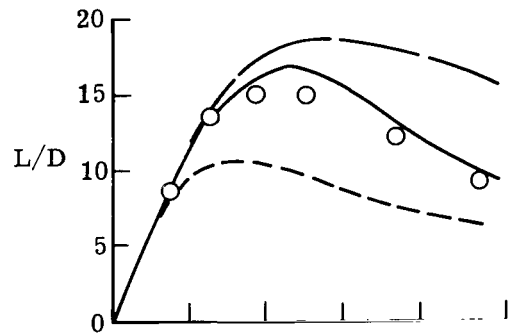
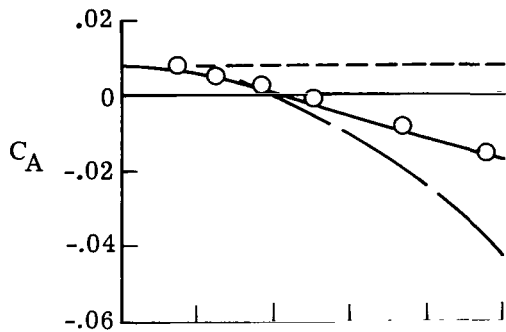


NACA 0005-63 Section
 $M = 0.25$, $R = 3.0 \times 10^6$

○ Experiment (ref. 8)

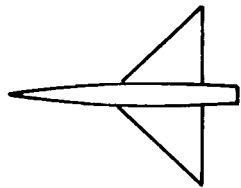
Theory

- No thrust
- Full thrust
- Present method



(b) $R = 3.0 \times 10^6$.

Figure 15.- Continued.

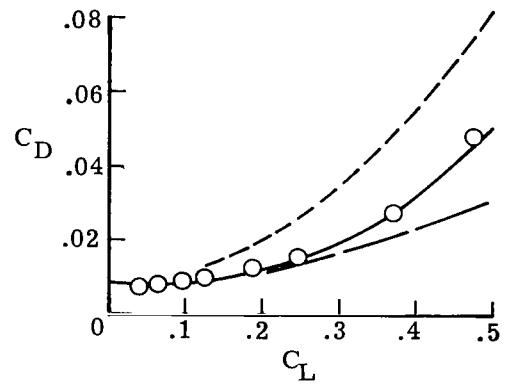
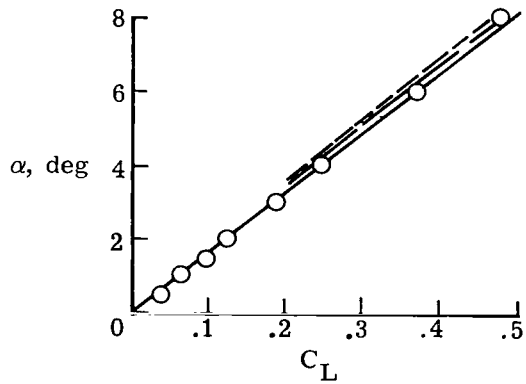
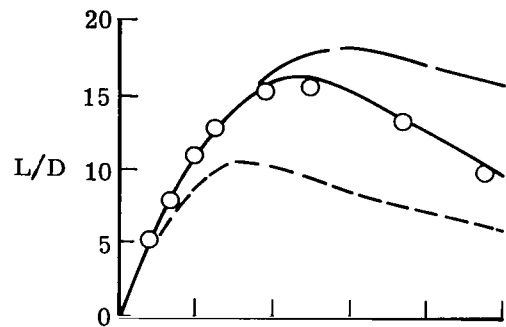
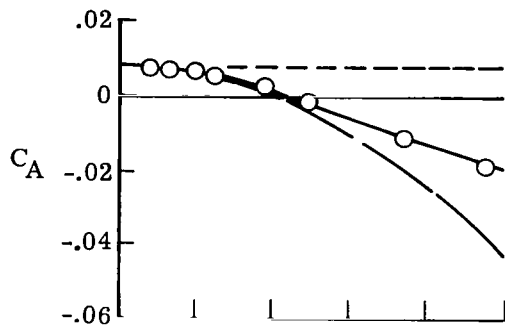


NACA 0005-63 Section
 $M = 0.25, R = 5.0 \times 10^6$

○ Experiment (ref. 8)

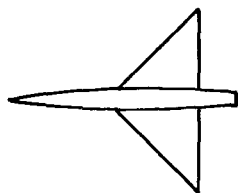
Theory

--- No thrust
 — Full thrust
 — Present method



(c) $R = 5.0 \times 10^6$.

Figure 15.- Continued.



NACA 0005-63 Section
 $M = 0.25, R = 8.0 \times 10^6$

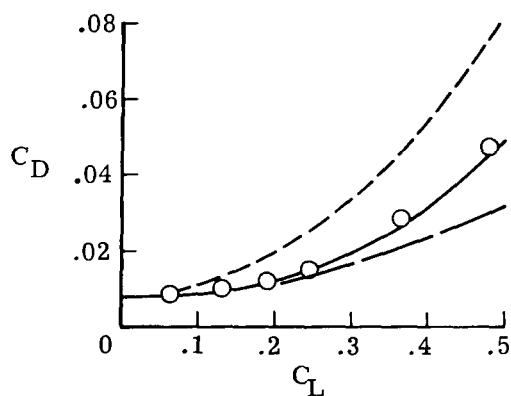
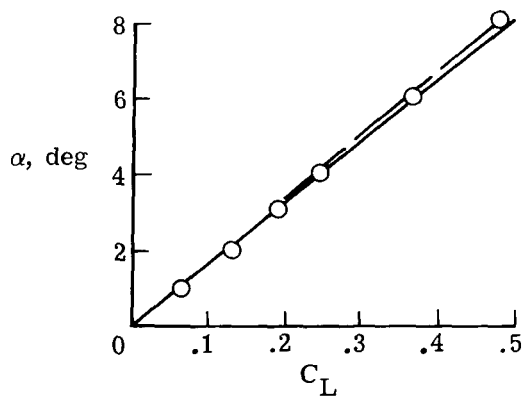
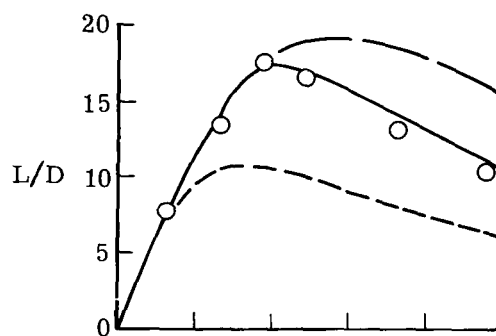
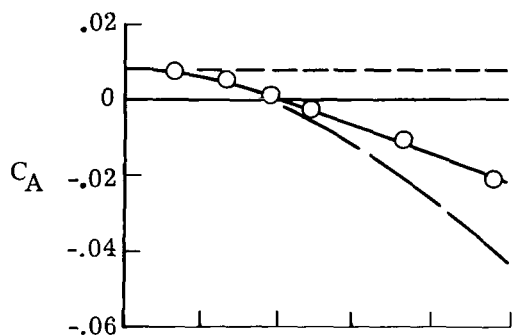
○ Experiment (ref. 8)

Theory

--- No thrust

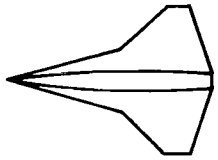
— Full thrust

— Present method



(d) $R = 8.0 \times 10^6$.

Figure 15.- Concluded.

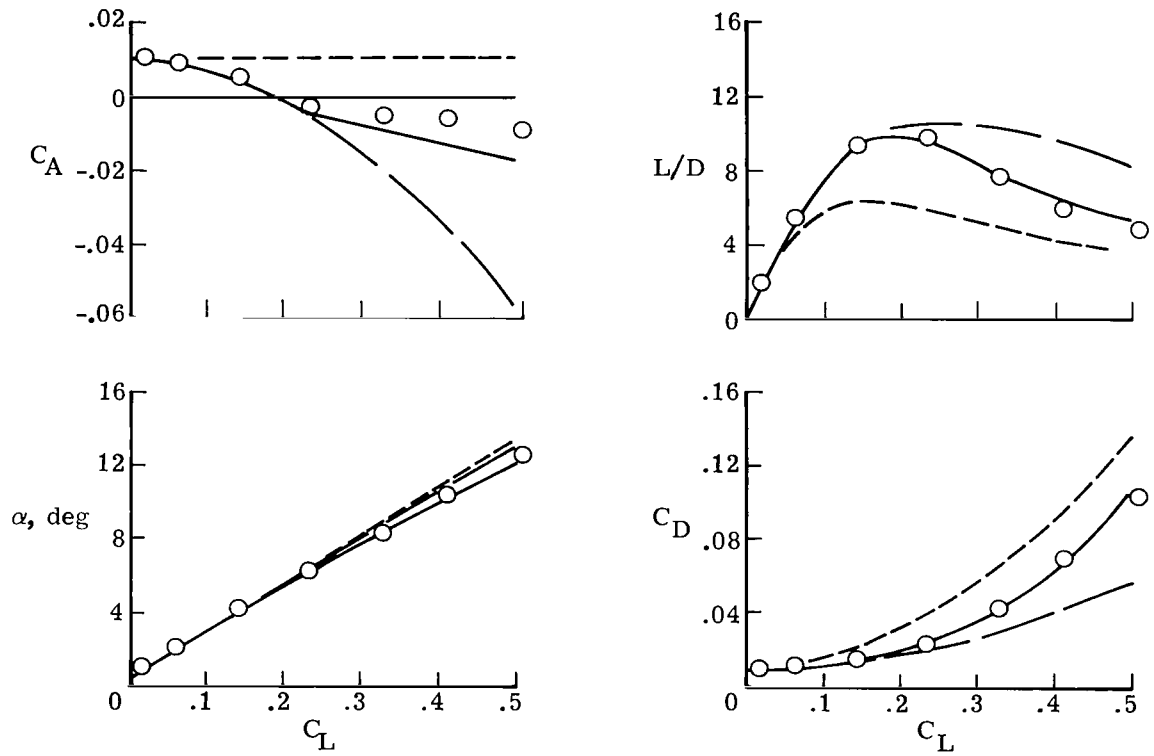


NACA 0008 Section
 $M = 0.60, R = 3.5 \times 10^6$

○ Experiment (unpublished)

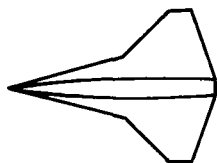
Theory

- No thrust
- Full thrust
- Present method



(a) $M = 0.60$.

Figure 16.- Comparison of theory and experiment for three Mach numbers; thick wing with cranked leading edge.

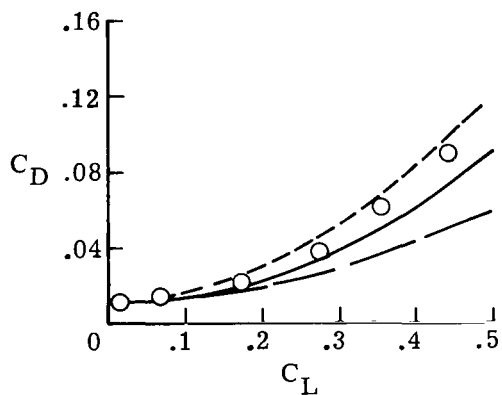
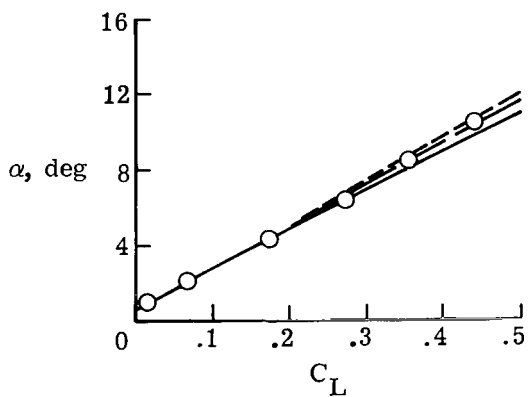
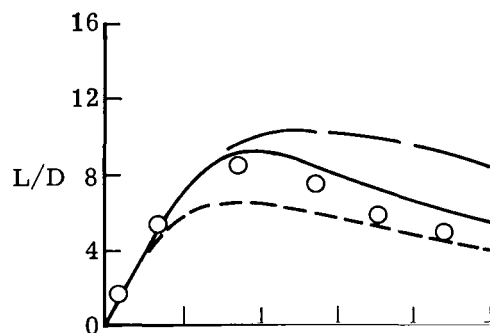
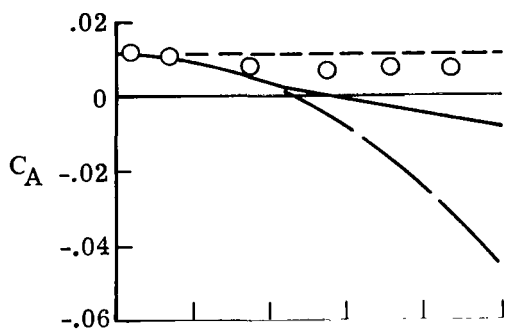


NACA 0008 Section
 $M = 0.90, R = 3.5 \times 10^6$

○ Experiment (unpublished)

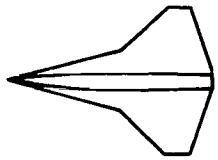
Theory

- No thrust
- Full thrust
- Present method



(b) $M = 0.90$.

Figure 16.- Continued.

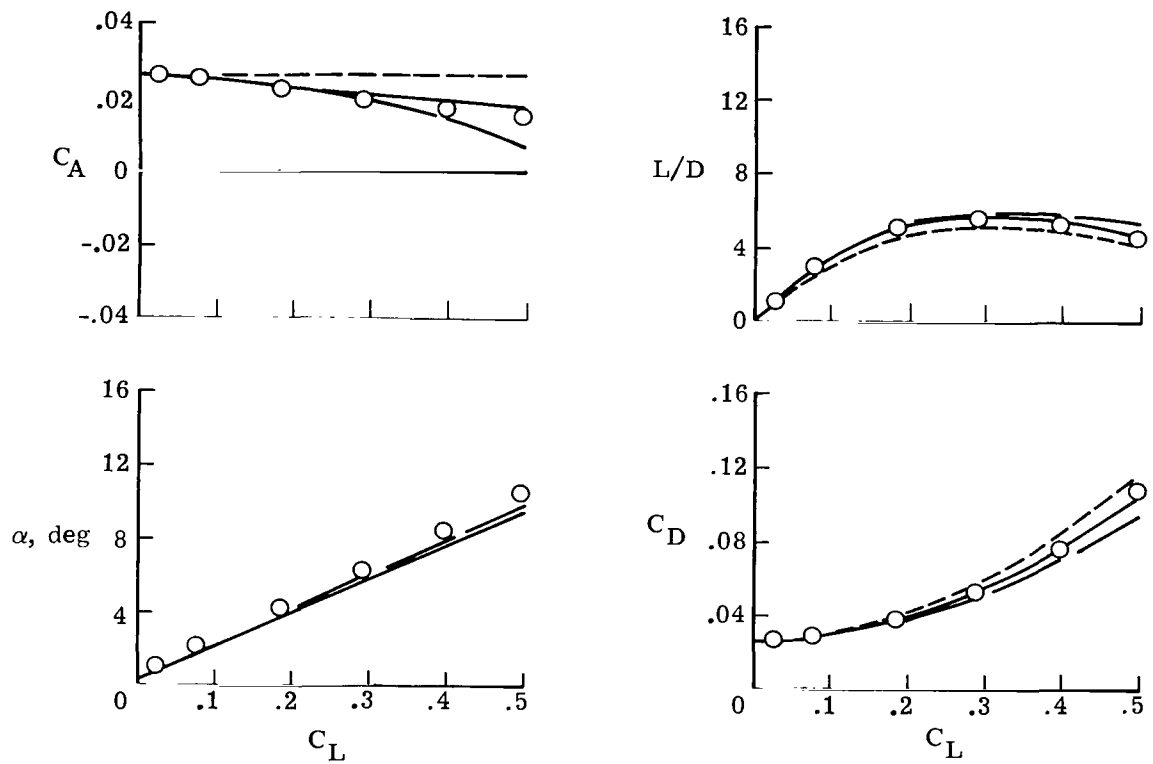


NACA 0008 Section
 $M = 1.2, R = 3.5 \times 10^6$

○ Experiment (unpublished)

Theory

--- No thrust
 - - - Full thrust
 — Present method



(c) $M = 1.2.$

Figure 16.- Concluded.

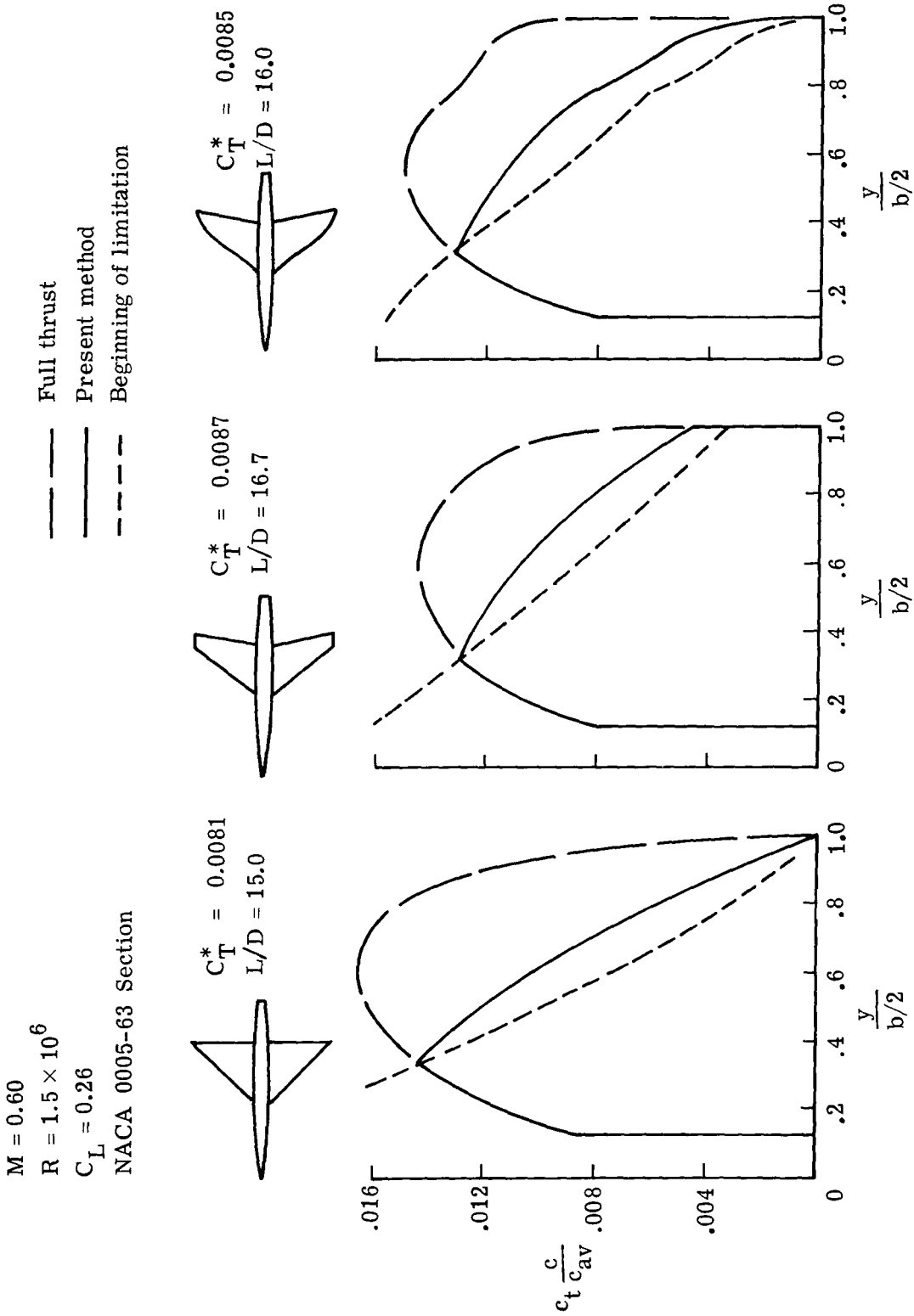
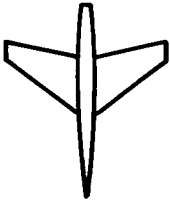


Figure 17.- Example of use of present method for wing planform design.



$M = 0.60$
 $R = 1.5 \times 10^6$
 $C_L = 0.26$

— Full thrust
 — Present method
 - - - Beginning of limitation

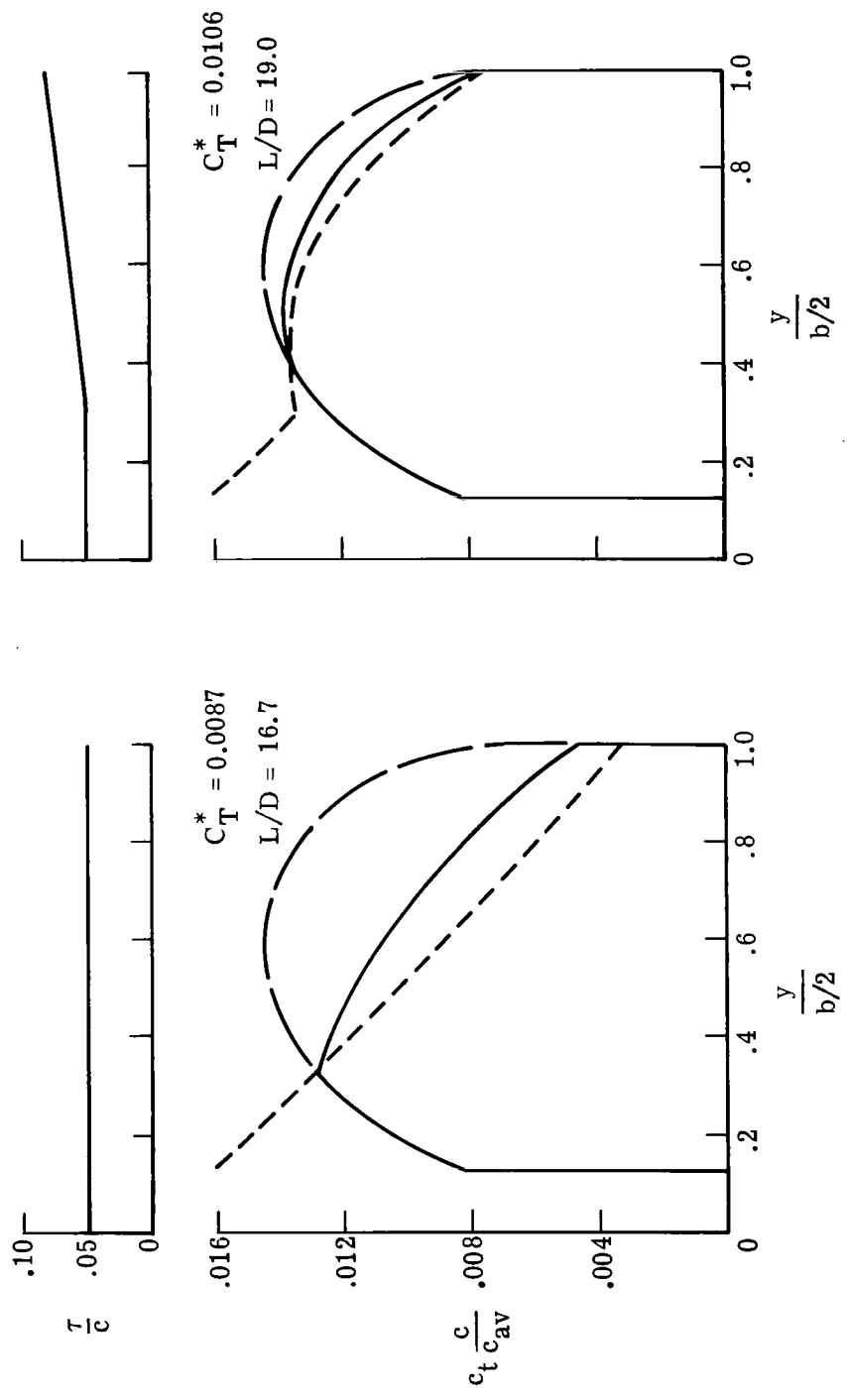


Figure 18.- Example of use of present method for airfoil section selection.

1. Report No. NASA TP-1500		2. Government Accession No.		3. Recipient's Catalog No.	
4. Title and Subtitle ESTIMATION OF ATTAINABLE LEADING-EDGE THRUST FOR WINGS AT SUBSONIC AND SUPERSONIC SPEEDS				5. Report Date October 1979	
7. Author(s) Harry W. Carlson, Robert J. Mack, and Raymond L. Barger				6. Performing Organization Code	
9. Performing Organization Name and Address NASA Langley Research Center Hampton, VA 23665				8. Performing Organization Report No. L-13032	
12. Sponsoring Agency Name and Address National Aeronautics and Space Administration Washington, DC 20546				10. Work Unit No. 517-53-43-03	
15. Supplementary Notes				11. Contract or Grant No.	
16. Abstract <p>A study has been made of the factors which place limits on the theoretical leading-edge thrust and an empirical method has been developed for the estimation of attainable thrust. The method is based on the use of simple sweep theory to permit a two-dimensional analysis, the use of theoretical airfoil programs to define thrust dependence on local geometric characteristics, and the examination of experimental two-dimensional airfoil data to define limitations imposed by local Mach numbers and Reynolds numbers. The applicability of the method was demonstrated by comparisons of theoretical and experimental aerodynamic characteristics for a series of wing-body configurations.</p>				13. Type of Report and Period Covered Technical Paper	
17. Key Words (Suggested by Author(s)) Leading-edge thrust Leading-edge suction Wing aerodynamic performance Wing lift and drag				14. Sponsoring Agency Code	
18. Distribution Statement Unclassified - Unlimited Subject Category 02					
19. Security Classif. (of this report) Unclassified		20. Security Classif. (of this page) Unclassified		21. No. of Pages 59	22. Price* \$5.25